J. Short
323-204

NSWC TR 79-143

THE EXPERIMENTAL ASPECTS OF COUPLING ELECTRICAL ENERGY INTO A DENSE DETONATION WAVE: PART I

BY DAVID L. DEMSKE

RESEARCH AND TECHNOLOGY DEPARTMENT

17 MAY 1982

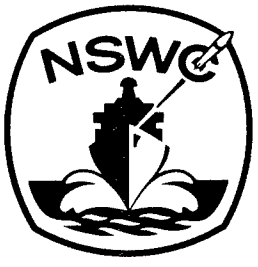

NAVAL SURFACE WEAPONS CENTER

Dahlgren, Virginia 22448 • Silver Spring, Maryland 20910

UNCLASSIFIED

SECURITY CLASSIFICATION OF THIS PAGE *(When Data Entered)*

REPORT DOCUMENTATION PAGE		READ INSTRUCTIONS BEFORE COMPLETING FORM
1. REPORT NUMBER NSWC TR 79-143	2. GOVT ACCESSION NO.	3. RECIPIENT'S CATALOG NUMBER
4. TITLE *(and Subtitle)* THE EXPERIMENTAL ASPECTS OF COUPLING ELECTRICAL ENERGY INTO A DENSE DETONATION WAVE: PART I		5. TYPE OF REPORT & PERIOD COVERED April 1977-September 1979 Technical REport 6. PERFORMING ORG. REPORT NUMBER
7. AUTHOR*(s)* David L. Demske		8. CONTRACT OR GRANT NUMBER*(s)*
9. PERFORMING ORGANIZATION NAME AND ADDRESS Naval Surface Weapons Center White Oak, Silver Spring, Maryland 20910		10. PROGRAM ELEMENT, PROJECT, TASK AREA & WORK UNIT NUMBERS 61153N; SR024-02-003/22128
11. CONTROLLING OFFICE NAME AND ADDRESS		12. REPORT DATE 17 May 1982 13. NUMBER OF PAGES 66
14. MONITORING AGENCY NAME & ADDRESS*(if different from Controlling Office)*		15. SECURITY CLASS. *(of this report)* Unclassified 15a. DECLASSIFICATION/DOWNGRADING SCHEDULE

16. DISTRIBUTION STATEMENT *(of this Report)*

Approved for public release; distribution unlimited.

17. DISTRIBUTION STATEMENT *(of the abstract entered in Block 20, if different from Report)*

18. SUPPLEMENTARY NOTES

19. KEY WORDS *(Continue on reverse side if necessary and identify by block number)*

005500 Electricity and Magnetism; 001600 Ammunition, Explosives, and Pyrotechnics; Electromagnetic Fields; Detonation Wave; Explosives; Resistive Heating; Shock Waves

20. ABSTRACT *(Continue on reverse side if necessary and identify by block number)*

An investigation into the effects of coupling 108KJ of electrical energy into the region behind a dense detonation front is considered. The purpose is to overdrive the detonation velocity.

This is an interim report discussing the experimental considerations and arrangement for accelerating the 8.8 mm/μsec detonation velocity of PBX9404, by injecting a 0.17 Megamp current pulse into the conductive zone

DD FORM 1 JAN 73 1473 EDITION OF 1 NOV 65 IS OBSOLETE
S/N 0102-LF-014-6601

UNCLASSIFIED

SECURITY CLASSIFICATION OF THIS PAGE *(When Data Entered)*

20. (Continued)

of a detonating explosive. The stored, electrical energy from a variable, fast-switched storage inductor is selectively transferred into the partially-conductive region behind the detonation front, culminating in the increase of the reaction energy in the detonation process. The effects are principally of an ohmic-heating nature.

Streak camera diagnostics are employed to assess the extent to which electrical coupling can be effected in comparison to the theoretically established, 20% increase in detonation velocity. The details of experimental parameters influencing such interactions and the diagnostic techniquires currently employed are discussed.

FOREWORD

The work reported herein describes the developmental stages of an experimental facility to be used for investigating the effects of injecting a high current density into the dense detonation wave of a high explosive. The experiments represent a proof-of-principal effort where the electrical conductivity features of a detonating explosive are exploited for the purpose of augmenting a number of basic explosive properties such as detonation velocity, detonation pressure and the rate of energy release.

The work is being carried out in the Detonation Physics Branch of the Energetic Materials Division of the Research and Technology Department as part of the Independent Research Program; Task No. 211, and NAVSEASYSCOM; Energetic Materials (explosives) Research, Task No. SR0 24-02-003/22128.

J. F. PROCTOR
By direction

PREFACE

The author wishes to acknowledge the considerable contributions of the following individuals: S. A. Longas, for his assistance with electronic instrumentation; J. W. Watt, for his assistance with the design and fabrication of various mechanical components; Dr. P. DiBona for his assistance on setting up the optical instrumentation currently employed; Drs. E. Zimet and E. Toton for their theoretical discussions of various aspects of the experiment, and Dr. D. J. Pastine who suggested the basic concept. Also gratefully acknowledged are I. Vitkovitsky, R. Ford, and D. Conte of the Naval Research Laboratory, for the use of their explosive switching systems designs. The time Richard Ford took to discuss opening switches is especially appreciated. Bruce Freeman of Los Alamos National Laboratory made several instructive suggestions which in turn inspired the author to make a more diligent study of the ground and shielding schemes currently used in the pulse power environment indigenous to this facility. Finally, the author wishes to express his sincere appreciation to Dr. Jerry Forbes for his suggestions regarding completion of the final manuscript, and for his diligence in suffering through the arduous task of proofreading this report.

CONTENTS

ILLUSTRATIONS

TABLES

INTRODUCTION: PRELIMINARY EXPERIMENTAL CONSIDERATIONS

The General Background. An extensive effort is underway to transfer the stored electrical energy from a 108 kilojoule, (5kV) capacitor bank into the partially-conductive zone behind the dense ($\sim 10^{22}$ particles/cm^3) detonation front of an explosive reaction. The capacitor assembly provides a versatile and reusable device for these initial feasibility studies.

The principal objective is to couple a significant amount of this electrical energy into the explosive reaction in order to effect a 10-20% increase in the detonation velocity. The subsequent increase of the Chapman-Jouquet pressure is expected to be on the order of 20-40%.

Figure 1 is a schematic diagram portraying the features of the experimental arrangement. Briefly, the 108 kilojoules of energy stored in the capacitor bank (C) is released on the closure of the explosively-driven closing switch (C.S.) and transferred to a storage inductor L_s after which the bank is disengaged from the circuit via an opening switch (f). The use of the intermediary storage inductor is warranted by the LCR timing constraints associated with coupling into the high-resistive load typically characteristic of a detonating explosive's reaction zone.

On referring to Figure 1 (a) we can see that, during the inductor-energizing phase, the (unreacted) explosive (between electrode, E', E" in the Figure) functions in the capacity of a normally-opened dielectric switch; its primary purpose is to hold back current from the discharge circuit (b) until the inductor has attained a maximum current value of ~ 0.17 MA. About 5 μsec prior to the opening switch disruption the detonation event is initiated thus effectively establishing the closed LR-discharge configuration in Figure 1 (b). Upon initiation of the explosive, energy stored in L_s is rapidly transferred through the electrodes (~10 μs duration) and into the partially-conductive zone of the detonation as it propagates through the forward (unreacted) portion of the solid explosive. Since energy transmission from the capacitor bank is completely severed from the system prior to the transfer of power into the resistive detonation, all transferred energy is captured within the inductive-resistive portion of the network, and all energy is ultimately dissipated within the resistive load. The

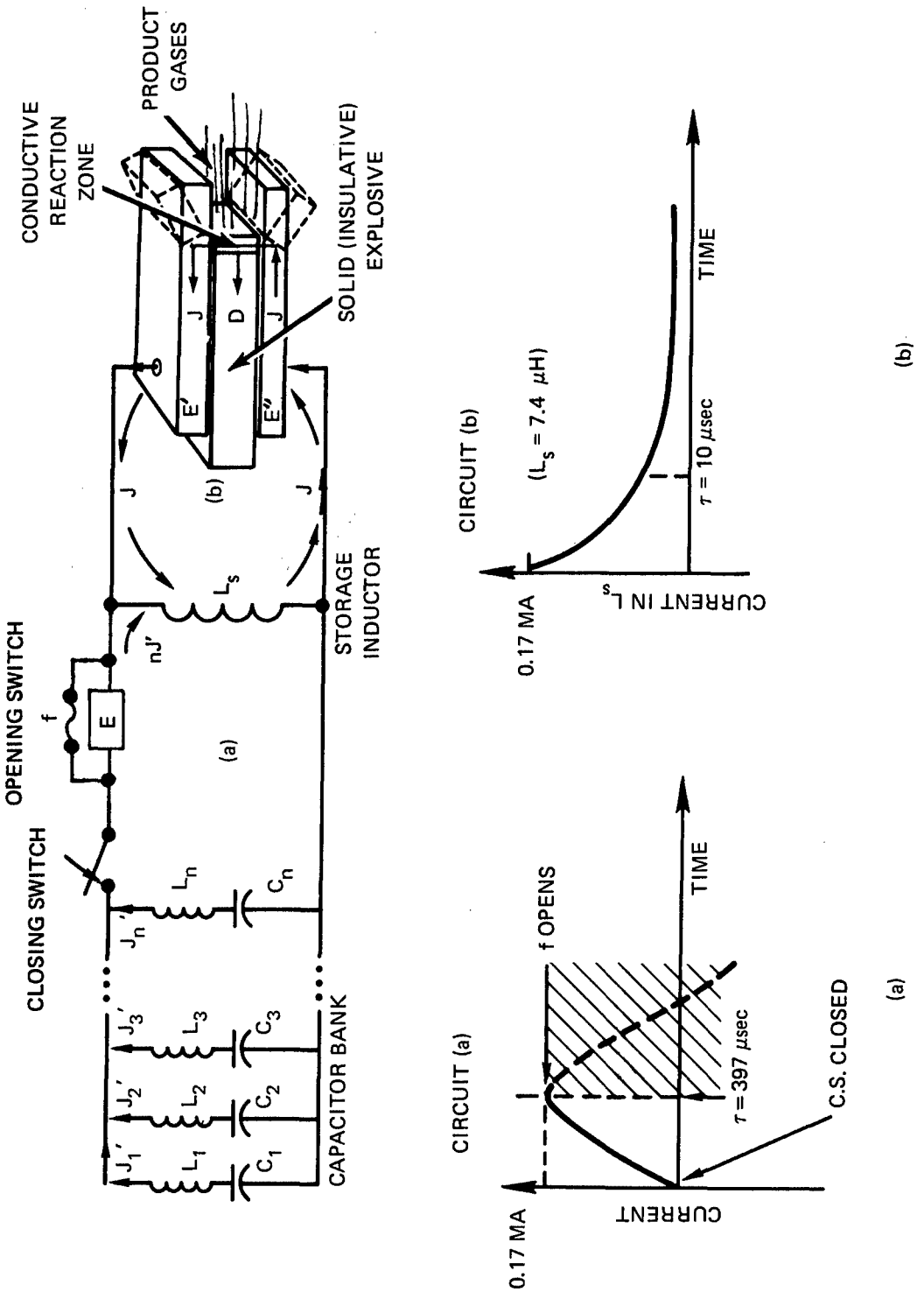

FIGURE 1 SCHEMATIC DIAGRAM OF THE PRELIMINARY EXPERIMENTAL ARRANGEMENT:
(a) NETWORK DESIGNATED FOR CAPACITIVE CHARGING OF THE STORAGE INDUCTOR: SWITCHES C.S. AND f ARE CLOSED; ONLY CIRCUIT (a) IS OPERATIONAL. ELECTRODES (E′, E″) ARE INSULATED FROM ONE ANOTHER BY THE SOLID EXPLOSIVE.
(b) NETWORK DESIGNATED FOR DISCHARGING THE STORAGE INDUCTOR INTO DETONATING EXPLOSIVE FOR A 10 μsec DURATION. SWITCH f IS OPEN, DISENGAGING CIRCUIT (a).

usual limitations of impedance matching are thereby circumvented since a highly efficient transfer of energy from the capacitor bank to the storage coil can be achieved.

The secondary explosive PBX 9404 (93% HMX) has initially been selected to provide the source of the detonation on which the electrical enhancement of detonation velocity (D = 8.8 km/s)[1] will be made. These effects are principally of an ohmic heating nature, and are characterized by the complex impedance $Z(R,\omega L_s)$, the enhancement effect being tantamount to increasing the reaction energy of the detonation process.

Primary experimental considerations are given to assessing the extent to which electrical coupling is effected, and to examining those significant transport properties involved with influencing such interactions. The details of the experimental arrangement and the diagnostic techniques currently employed are discussed.

Preliminary Experimental Aspects. The experiments represent a "proof-of-principal" attempt at achieving the transfer of a large current density (on the order of $\sim 10^5$ amp cm^{-2}) into the electrically conductive region immediately forward of the Chapman-Jouquet plane where the charge carrier density $n_e \sim 10^{18}$ cm^{-3}.[2] The width of this conductive region (~1-3 mm) is controlled by the chemical reaction time and correspondingly the temperature. Figure 2 depicts a qualitative profile of the electrical conductivity distribution in a reacting explosive. The more prominent features such as the relative location of the conductivity peak and the extreme exponential falloff in the near-to-far product zones have been experimentally substantiated.[3] The spatial distribution indicates the preferred current path and consequently implies information on the nature and extent of the coupling mechanisms involved. In particular, the effectiveness of coupling is far less significant if a substantial conductivity σ (e.g., $\sigma \leq 0.1$ mho cm^{-1}) exist in the detonation products. From a circuit analysis viewpoint where the conductive zone is simply regarded as a bulk resistive load, the current transfer rate is inversely proportional to the magnitude of $\langle\sigma(\xi)\rangle$, consequently dictating the particular network configurations which are

---

[1] Dobratz, B. M., "Properties of Chemical Explosives and Explosive Stimulants," Lawrence Livermore Laboratory Report No. UCRL-51319, Revision 1, 1974.

[2] Ershov, A. P., "Ionization During Detonation of Solid Explosives," Combustion, Explosion, and Shock Waves, pp. 798-803, November - December 1975.

[3] Walbrecht, E. E., "Dielectric Properties of Some Common High Explosives," PATM 1170, p. 1, April 1963.

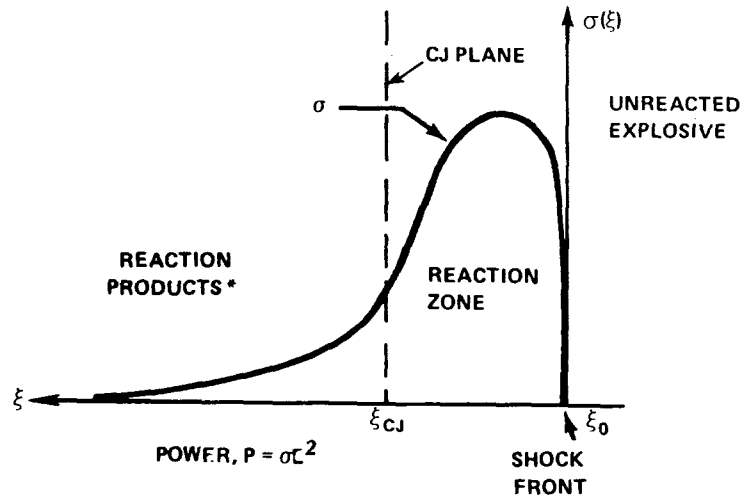

(a) A QUALITATIVE PROFILE OF THE ELECTRICAL CONDUCTIVITY AS A FUNCTION OF DISPLACEMENT INTO THE DETONATION WAVE FRONT.

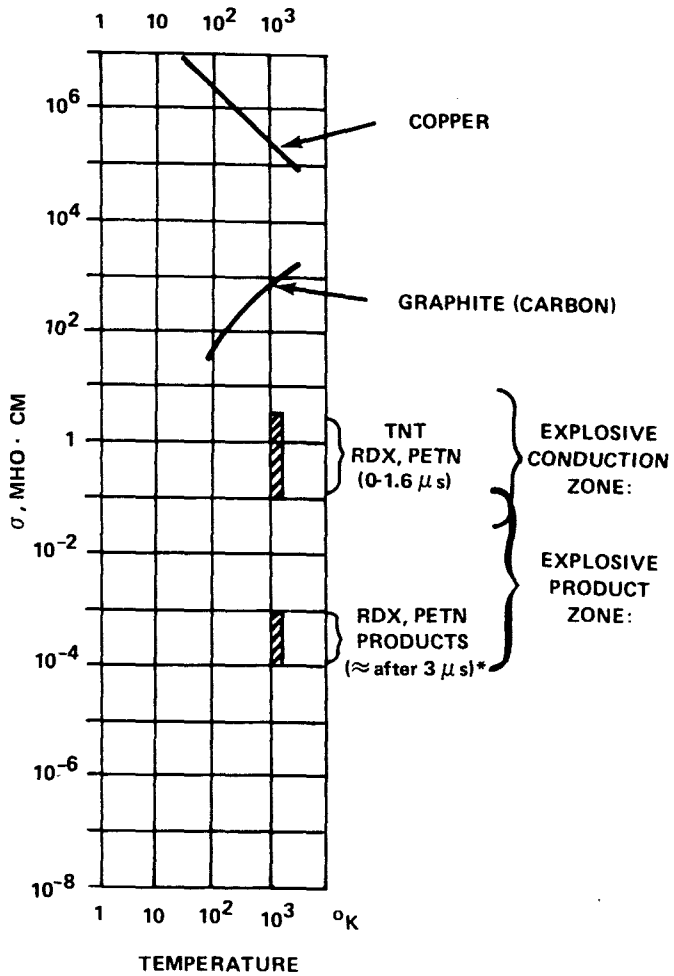

(b) INTRINSIC CONDUCTIVITY AS A FUNCTION OF TEMPERATURE; (REF 17)*

FIGURE 2 THE GENERAL FEATURES OF THE ELECTRICAL CONDUCTIVITY EXHIBITED IN A (ONE-DIMENSIONAL) DENSE DETONATION WAVE.

compatible with the time constraints imposed by the detonation velocity through a given electrode length. The discussion in a later section will show that for a given explosive's resistance these requirements are met by employing a simple LR circuit with the inductance L_S as an experimentally adjustable parameter. The I(t)R drop across the conduction zone defines the voltage requirements imposed on the storage inductor. In the course of disengaging the capacitor circuit from the inductor, microsecond switching across the inductor provides the necessary voltage required to drive the current through the resistive load. In this instance the rate determining component is the commutation rate of a paralleled exploding wire otherwise employed to relax the voltage stress across the opening switch. The effects of this current commutation, generating voltages in excess of 10^2kV, point up the danger of overvoltaging various network components and in particular to the explosive itself. Conversely, it defines the possible current limiting conditions unless involved modifications to the electrodes are made. The concern over voltage breakdown whether by channeling through an unreacted portion of the explosive itself, or by arcing in the tenuous product region because of the extended conductivity tail, go into the considerations of the particular explosive being investigated. For a given set of network conditions it is necessary that the breakdown voltage of the solid explosive be greater than any induced voltages incurred during the course of energy transfer or premature breakdown at the explosive may ensue. In the same context, the switching assembly must be capable of recovering long enough to relax to the condition where restrike back across the switch is no longer a danger.

Both electrical conductivity and voltage breakdown are intimately incorporated in the considerations of the diagnostic setup. Enhancements resulting in a 10-20% increase of detonation velocity are shown to be theoretically feasible;[4] the actual enhancement effect will be measured by employing fast photography techniques to measure velocity changes. The spatial resolution afforded under existing streak camera techniques warrants that the electrical energy be roughly comparable to that of the chemical energy released by the explosive; in other words, that some ratio of these two,

$$\beta \equiv \frac{\text{Electrical Energy Input}}{\text{Chemical Release Energy}} \sim 1. \qquad (1)$$

Unfortunately, in attempting to optimize this stipulation it is found that the limiting constraints are: 1) breakdown voltage requirement and 2) the coupling interaction time. In the former case, there must be a sufficient amount of explosive to prevent breakdown across the electrodes during the course of switch closure. The electrode spacing requirement is even more stringent when the concern over

[4]Toton, E. T., "High Explosive Detonation and Electromagnetic Interaction," NSWC TR 79-205.

arcing in the reaction products exists. The second constraint arises out of the realization that the coupling interaction be maintained long enough to provide for a measurable detonation track. For PBX 9404 with a detonation velocity of 8.8 km. sec.$^{-1}$, it is found that 5 cm. is about the minimum length needed to establish an acceptable measurement.

The electrodes currently in use are designed to contain a 113.5 g, 10 cm long explosive sample, and are spaced 0.7 cm apart. The chemical energy releases is ~500 kilojoule. On the assumption that the optimum amount of electrical energy is transferred, $\beta \sim 0.09$ for the present experimental arrangement.

ELECTRICAL CONDUCTIVITY IN DENSE DETONATIONS

The General Significance to Energy Coupling. The electrical conductivity distribution $\sigma(\xi)$ plays a significant role in determining: (a) the extent of direct ohmic heating in the detonation, (b) the extent of inductive heating in the detonation, and (c) the LR circuit time-constant characterizing the rate of energy transfer to the detonation wave itself. These features are considerably more evident when examined in the context of the Fourier analyzed LR current response where the first two Fourier expansion coefficients represent the dominant energy coupling mechanisms. Both of these terms are ultimately responsible for the ohmic dissipation mechanism in the conductive region of the detonation wave, and both intimately depend on the spatial conductivity distribution $\sigma(\xi)$. Details of the LR circuit response are addressed later. Here a brief account is given of the physical nature of $\sigma(\xi)$ as applied to the coupling mechanism as a whole. The displacement relative to the shock front is defined as ξ (see Figure 2a).

For explosive reactions producing a low carbon content, the nominal conductivity values will generally span a range of 0.3-5 mhos cm^{-1}.[5] Table 1 includes the measured values for a

[5] Brish, A. A., Tarasov, M. S., and Tsukerman, V. A., "Electric Conductivity of the Explosive Products of Condensed Explosives," Soviet Physics JETP, Vol. 37, (10), No. 6, pp. 1095-1099, June 1960.

TABLE 1 MEASURED VALUES OF THE ELECTRICAL PROPERTIES OF VARIOUS EXPLOSIVES

Explosive	Mass Density (g/cm^3)	Det'n Speed (km/sec)	Average Electrical Conductivity[a] (mhos/cm)	Investigator or Information Source	Breakdown Voltage[b] (Volts)	Distance Between the Electrodes(cm)	Investigator or Information Source
		A. DETONATION WAVE OF EXPLOSIVE			B. UNREACTED EXPLOSIVE		
85% PETN	1.5	7.2	0.30	Ref. 12, 32			
85% PETN	1.7	7.2	0.60; 0.60	Ref. 12, 32			
85% PETN	0.8[c]	--	0.13	Ref. 5			
Comp B	1.6	7.8	0.93-1.07[d]	Ref. 31	10,200 ± 420	0.20	J. W. Forbes, NSWC Data
Pentolite	1.6	7.5	0.56-1.12[e]	Ref. 31			
Nitromethane	1.1	6.2	1.6	Ref. 32			
PBX-9404	1.81	8.8	--	Ref. 1	>24,000	00.20	J. W. Forbes, NSWC Data
" +.24Ce[f]	--	--	11	Ref. 33, 34			
Hexogen (RDX)	0.8[c]	6.2	0.23	Ref. 5			
TNT/Hex[g]	0.8	5.7	1.0	Ref. 5	5000	0.10	Reference 3
TNT/Hex[g]	1.64[h]	7.7	5.0	Ref. 5			
TNT	0.8[c]	4.5	4.0	Ref. 5	3500-4000	0.10	Reference 3

(a) In Conductance Zone, Under Low Current Conditions.
(b) A Bulk Measured Value (Dielectric Stress).
(c) Powdered Form.
(d) Internal, Double Probe Meas.
(e) Surface Measurements (from 3 Different Probes).
(f) PBX-9404 Seeded with 24% Cesium Picrate.
(g) 50% TNT and 50% Hexogen.
(h) Molded Form - an "Alloy" of the Composition.

number of such explosives, but under rather low current density conditions.[6,7,8,9] Unfortunately, the conductivity profile for PBX9404 has not been measured.* However, a review of a number of experimental papers on similar explosives[5,10,11] strongly infers that the low current peak value will fall somewhere in the general range of those given in the table. The mean conductance value will be established in the course of our experiment by monitoring the voltage-current profile under the high current density conditions which are more applicable to our particular experiments.

The General Features of a Partially Ionized Fluid. Ershov[2] and Zubkov, Luk'yanchikov, and Novoselov[10] have investigated a number of general electrical conductivity features under low current densities, i.e., on the order of 50 A/cm^2 - specifically for P.E.T.N. and Hexogen (RDX). Investigations of electrical properties in explosives indicate that the conductive region in a reactive explosive medium is typically characterized by a 3,500°K, partially-ionized, degenerate fluid containing an exceedingly high density of neutral molecules (i.e., $n_o \sim 10^{22}$ particles/cm^3).[2] At these densities and temperatures the electrical transport properties are characteristically attributed to a collision-dominated mechanism. Owing to the significant mass difference between ions and electrons ($m_e/m_i \ll 1$) and to the predominance of electron-neutral collisions (where $\nu_{e,n} \approx 10^{15}$/sec), the electrons are expected to be the dominant current carriers. For the ~3.6kV/cm field appearing in the electrode gap, it can be inferred that electron current mobilities in excess $10^5 \frac{cm^2}{V \cdot sec}$ occur.

---

[6] Jameson, R. L., Lukasik, S. J., and Pernick, B. J., "Electrical Resistivity Measurements in Detonating Composition B and Pentolite," Journal of Applied Physics, Vol. 35, No. 3, Part 1, p. 714, March 1964.

[7] Hayes, B., "On Electrical Conductivity in Detonation Products," Fourth International Symposium on Detonation, p. 595, 1965.

[8] Jones, M. S. and Blackman, V. H., "Parametric Studies of Explosive Driven MHD Power Generators," Symposium on the Engineering Aspects of MHD, Vol. 2, August 1964.

[9] Jones, M. S., McKinnon, C. N., and Blackman, V. H., "Generation of Short Duration Pulses in Linear MHD Generators," Proceedings of Fifth Symposium on the Engineering Aspects of MHD, MIT, April 1964.

[10] Zubbov, P. I., Luk'yanchikov, L. A., and Novoselov, B. S., "Electrical Conductivity in the Detonation Zone of Condensed Explosives," Combustion, Explosion, and Shock Waves, pp. 253-256, June 1971.

[11] Allison, F. E., "Detonation Studies in Electric and Magnetic Fields," Proceedings of the Conference on Megagauss Magnetic Field Generation by Explosives and Related Experiments, 21-23 September 1965.

* PBX9404 (93% HMS) was initially selected on the basis of its very high breakdown voltage characteristics and its well established detonation properties (cf. Table 1).

Where $\nu_{e,n}$ provides the dominant momentum transfer mechanism,[2,12,13] the current mobility is generally expressed in terms of this collision frequency by[12]

$$\mu_e = \frac{|e|}{m_e \nu_{e,n}} \; ; \; \nu_{i,e}, \nu_{i,i} << \nu_{e,n}. \qquad (2)$$

where $\nu_{i,i}$ defines the ion-ion collision frequency for the momentum transfer mechanism. For these situations where the degree of ionization is relatively low, the resistivity $\eta(\xi)$ is primarily determined by electron collisions with the neutral molecules.* The degree of ionization, in turn, depends on the electron temperature and the collision cross-sections involved.[13] At these electron densities the reaction zone of an explosive detonation is "too cold" to technically be considered a plasma. Consequently, analysis of electrical conductivity properties, approached from the usual "collective-field effect" typically associated with the tenuous plasmas, should be viewed with some trepidation.**

Ershov's analysis is primarily predicated on the tacit conditions of low electric fields and widely-spaced collisions (i.e., a rarefield gas) in the one limit, and of low electric fields and an extremely degenerate electron gas (i.e., kT <<3 ev) in the other.[2,15] For dense, weakly ionized fields subjected to high electric current densities, a conductivity analysis must generally include the "persistance-of-velocity" effects, where the charge particles retain some memory of past collisions.[12] The difficulty ultimately resides in attempting to calculate the electron drift velocity distribution $\langle W_e \rangle$ needed to establish the electric conductivity.

---

[12] Reif, F., Statistical and Thermal Physics, McGraw-Hill Book Company, New York, pp. 531-534, pp. 580-582, 1965.

[13] Dreicer, H., "Electron Collision Phenomena in Partially Ionized Gases," Phys. Rev. 117, p. 329, 1960.

[14] Krall, N. A., Trivelpiece, A. W., Principals of Plasma Physics, McGraw-Hill Book Co., Inc., New York, p. 57, 1973.

[15] Zel'dovich, Ya. B. and Raizer, Yu. P., Physics of Shock Waves and High-Temperature Hydrodynamic Phenomena, Vol. 1, Academic Press, Inc., pp. 218-219, pp. 229-232, 1966.

* It can be shown that if "self-similar" collisions were frequent enough, i.e., $\nu_{i,i}$ (or $\nu_{e,e}$) $\approx \nu_{e,n}$, they would not effect the electrical conductivity since such collisions merely exchange roles in the mobility terms; the mobility contributions (where $\mu_{\alpha\alpha} \equiv \frac{|e|}{m_\alpha \nu_{\alpha\alpha}}$) have been shown to be negligible in comparison to Eq. 2 above.[12,13]

** In general, the plasma "collective field" conditions stipulate that plasma parameter g<<1 where $g = 8 \times 10^{-3} \; (n_e^{1/2}/T^{3/2}{}_{^\circ K})$. For our detonation process, this condition is not satisfied at 3500°K. (Even for $n_e \sim 10^{17}$/cm, g ~ 12.).[14]

In the rest frame of the detonation the current mobility, Equation (2), is related to the applied electric field in the electrode gap by

$$\langle \vec{W}_e \rangle = \mu_e \vec{E} \text{. where } \vec{E} \text{ is the field intensity in} \qquad (3)$$

the gap $\left(|\vec{E}| = \frac{d\phi \text{ across electrodes}}{\text{electrode spacing}} \right)$, where $d\phi$ is the potential difference. The corresponding current density flowing across the explosive's conductive channel is

$$\vec{j} = - n_e(\xi) e \langle \vec{W}_e \rangle \qquad (4)$$

The actual mathematical analysis is a rather involved topic and will not be taken up here. Dreicer's paper[13] perhaps best sets the stage for pursuing the quantitative aspects in more detail.

Direct Ohmic Heating Effects. Since it will be primarily the resistivity distribution $\eta(\xi)$ which limits the current flow through the detonation, in the detonation frame of reference, upon inserting Equation (3) into Ohm's law

$$\vec{j}(\xi) = n_e(\xi) |e| \mu_e \vec{E} \, , \qquad (5)$$

and, by Equation (2)

$$\vec{j}(\xi) = \{ n_e(\xi) \, e^2 / (m_e \nu_{e,n}) \} \vec{E} \, . \qquad (6)$$

Here $n_e(\xi)$ is the electron number density, spatially distributed throughout the conductive zone, and defined relative to the position of detonation front ξ_o. Generally, for any conductive fluid moving with a velocity $\vec{D}$ the convective current density is described by the expression[16,17,18]

$$\vec{j}_c = \vec{j} + n_e \vec{D} \, . \qquad (7)$$

It is readily shown below that only the conduction current $\vec{j}$ effects joule heating term ηj^2; this increases the temperature

---

[16] Jones, M. S., Bangerter, C. D., Peterson, A. H., McKinnon, C. D., "Explosive Magnetohydrodynamics," AFAPL-TR 67-64, pp. 67-72, August 1967.

[17] Jackson, J. D., Classical Electrodynamics, 2nd, Ed., John Wiley and Sons, Inc., pp. 471-479, 1975.

[18] Sutton, G. W. and Sherman, A., Engineering Magnetohydrodynamics, McGraw-Hill Book Co., New York, pp. 125-209, and pp. 300-304. 1965.

of the conductive zone via direct ohmic dissipation. By Equation (2) and Equation (6) and $\eta(\xi)$ defined by the expression

$$\eta(\xi) = \frac{m_e}{e^2}\left(\frac{\nu_{en}}{n_e(\xi)}\right) , \tag{8}$$

the joule heating term is obtained. The energy dissipation in a given time δt is

$$q \simeq 10^{-8}\left(\frac{\nu_{e,n}}{n_e}\right) j^2.\delta t. \tag{9}$$

Referring to Gauss' Law (or Poisson's equation) gives $\vec{\nabla} \cdot \vec{E} = \frac{e}{\varepsilon} \cdot (n_i - n_e)$. On the assumption that E varies unappreciably over the electrode gap W, the charge density n_e in Equation (7) scales like

$$n_e \simeq \varepsilon_o E/W \tag{10}$$

The convective (maximum) current density term $n_e\vec{D}$ divided by the conduction current density $\sigma\vec{E}$ gives

$$\frac{n_e D}{\sigma E} \simeq \frac{(\varepsilon_o E/W)D}{\sigma E} = \frac{\varepsilon_o D}{\sigma} . \tag{11}$$

For conductivities typically exhibited by explosives (Table 1),

$$\sigma \simeq 10^2 \text{ mho/m}, \quad W \simeq 0.7 \times 10^{-2}\text{m},$$

$$\varepsilon_o \simeq 10^{-11} \text{ farad/m}, \quad D = 8.8 \times 10^2 \text{ m/sec},$$

and so Equation (11) gives $\frac{\varepsilon_o D}{\sigma W} \simeq 10^{-8}$. Consequently, for this situation the contribution from the detonation propagation term n_eD to convective current flow in Equation (7) is negligible in comparison to the conduction current given by Equation (6). The energy dissipation in a conductive fluid itself when a given current flows in it, whether expressed by Equation (9) or for the moving detonation wave (relative to the lab frame), cannot depend on the motion of the conductive system.[19] The rate of evolution of joule heating per unit volume is still given by the same expression,

[19] Landau, L. D. and Lifshitz, E. M., The Classical Theory of Fields, 2nd. Ed., Addison-Wesley Publishing Co., Inc., Reading, Mass., pp. 101-108, 1962.

$q = (\eta j^2)\delta t$. However, as the detonation front proceeds through the electrode pair, i.e., in the "laboratory frame," the measured "effective" electric field is[20]

$$\vec{E}' = \vec{E} + (\vec{D} \times \vec{B})/c \tag{12}$$

It is this field that produces the conduction current $\vec{j}$ $(=\sigma(\varepsilon)\vec{E}')$ and consequently the joule heating rate per volume is

$$(\eta j^2)\delta t = (\vec{j}\cdot\vec{E}')\delta t^* = \left[\vec{j}\cdot\left(\vec{E} + \frac{\vec{D}\times\vec{B}}{c}\right)\right]\delta t \quad \text{where} \tag{13}$$

B is the magnetic field induced by current flow in the electrodes. If dv is the volume of the conduction zone being heated by this inductive effect, the additional heat evolved due to the effect of the second term in bracketed expression is

$$q' \equiv \delta t \int \vec{j} \cdot \left(\frac{\vec{D}\times\vec{B}}{c}\right) dv \quad , \tag{14}$$

This is small for the electrode configurations presently being considered** for the detonation velocities and electric conductivities indigenous of explosives. The details of this induced ohmic heating effect are elaborated on in the next Section, and Appendix A. The first term in the bracketed expression, Equation (13), can be integrated over the reaction zone volume, then summed over each of the progressive time increments δt to give the amount of heat injected into the detonation. At each δt time step

$$q = \int \vec{j}\cdot\vec{E}dV = -\int (\vec{j}\cdot\vec{\nabla}\Phi)dV \quad . \tag{15}$$

j,$\Delta\Phi$ and dV are all experimentally obtainable quantities. The potential gradient across the electrode pair can be monitored in time by employing standard high voltage probe techniques, and the current flow through the electrode pair is measured by use of a modified Rogowski coil. Consequently, the amount of heat in the

---

[20] Landau, L. D. and Lifshitz, E. M., Electrodynamics of Continuous Media, Addison-Wesley Publishing Co., Inc., Reading, Mass., p. 197-212, 1960.

* The work done per unit time per unit volume by the force field $\vec{F} = e\int \vec{E}'n_e dv$ moving current carriers in the conduction zone results in evolution of heat and increases the entropy of the zone volume dv by $\frac{dq}{T}$.

** Some electrode configurations where inductive heating can be of some significance (e.g., helical configurations) are readily conceivable.

detonation medium per unit time, for each δt, over the volume of the conductive zone results in $q = \Sigma_k \phi_k \delta_k (t)$ for each time step δt. With the subsidiary condition of conservation of charge (div $\vec{j} = 0$), we can experimentally get

$$\int \vec{j} \cdot \vec{E} dV = \int (\eta j^2) dV \quad , \tag{16}$$

and hence the spatially-averaged resistivity for current can be determined.

Induced Ohmic Heating Effects. On taking the curl of Equation (12), with $E' = \eta j'$ and inserting Faraday's Law of Induction for the $(\nabla \times E)$ term, we get the expression[20] (reference is made to Appendix A for the algebraic details),

$$\frac{\partial \vec{B}}{\partial t} = \frac{\eta}{\mu_o} \vec{\nabla}^2 B + \vec{\nabla} \times (\vec{D} \times \vec{B}), \text{ (RMKS units)}. \tag{17}$$

The magnetic Reynolds number R_m represents an indication of how effective the interaction due to diffusion of the magnetic field lines are.

For our dense detonation situation (Appendix A),

$$R_m \equiv \frac{\mu_o D \ell}{\eta} \tag{18}$$

or

$R_m \sim 10^{-8}$ for $\eta \sim 10^3$ $\Omega \cdot m$, $D = 8.8 \times 10^3$ m/sec, and conduction zone length $\ell = 1.5 \times 10^{-3}$ m. τ_B, the time it takes for the B-field to dissipate into joule heat, is given by

$$\tau_B = \mu_o \sigma L^2 \quad \mu\text{sec}, \tag{19}$$

where L is the electrode length. With τ_D defined as the detonation time-of-flight (L/D), we see that there is sufficient time for annihilation of the magnetic flux lines to produce ohmic heating, i.e.,

$$N \equiv \frac{\tau_B}{\tau_D} << 1. \tag{20}$$

However for the low inductance electrode configuration, or (more significantly) for the low current densities which are available for this experiment the energy release is about 10^3 smaller than that of the chemical release energy. Consequently, q' is a negligible quantity for our conditions of D and η, and for the electrode configuration which is currently employed (cf. Equations (A.14), (A.15).

BREAKDOWN VOLTAGE CHARACTERISTICS

In the Unreacted Explosive. Preliminary design features of the experiment had to address the problem of voltage stand-off capability in various explosives. For PBX 9404 (94% HMX), 2 mm thick samples had been electrically stressed in excess of 24 kV without showing indications of initiation or voltage breakdown (cf., Table 1).

For nearly instantaneous interruption of the LC circuit configuration, the voltages generated are, in principal, determined by the magnetic field diffusion rate across the storage inductor. In actual practice however, the rate determinant process is governed by the opening switch response time. To prevent either the possibility of voltage overstressing at the opening switch or premature breakdown at the explosive (also due to overvoltage), an understanding of the particular switch assembly being employed is necessary. Also, to avoid prolonged discharge across the switch during the highest voltage level incurred under the circuit interruption impulse, an exploding wire fuse is employed in parallel with it; this has to be properly adjusted to relax the high voltage stress generated in the course of current switching.

During the inductor discharge phase, the peak voltages across the explosive coincides with the peak current; the induced voltages generated in the course of switching must satisfy the restriction where

$$V_b > \sum_j L_j \frac{dI}{dt} ,$$

or premature breakdown at the explosive may occur. Here

$V_b \equiv$ the solid explosive's breakdown voltage,

$L_j \equiv$ The equivalent network inductance, including the storage inductance.

Depending on the exploding wire length and material characteristics, the microsecond switching action generates voltages in excess of 100 kV.

In the Detonation Products. The possibility of current channeling through the product gases primarily depends on the magnitude of the conductivity there. Generally, this is expected to be very low in the product gaseous region. Korol'kov et. al. have measured high voltage breakdown in the low carbon level detonation products of PETN and RDX type explosives.[21,22] The values for voltage breakdown in these reaction products are found to be comparable to those generally associated with solid dielectrics. Korol'kov's experimentally observed dielectric strength values for RDX are above 65 kV for a 0.5 mm gap at about 14-34 mm behind the shock front. This would imply that there exist nearly a 200 kV holdoff voltage in about the same range of the product zone for the 1.6 cm electrode gap containing the PBX 9404 products gases.* Reference is made to Figure 3.[21,22] By virtue of these observed increases in dielectric strength during the 1.7-4.0 microsecond interval behind the shock front, it is felt that arcing probably will not occur. Breakdown in the far detonation product zone would rob the enhancement process of the otherwise preferential channeling of current through the reaction-to-near product zone where it is most effective. The object is to maintain the voltage across the product gases sufficiently low enough as to benefit from this low conductivity feature of the product zone. To further retard the tendencies toward arcing in the product zone, the copper electrodes have been put through a special tempering treatment process which allows them to flare outward without early tearing ahead of the reaction products as the shock front moves through them, subsequently increasing the electrode separation and lessening chances for high voltage breakdown.

A PRELIMINARY CIRCUIT ANALYSIS OF THE TWO LOOP NETWORK

Figure 1 shows an LCR circuit using a slow bank (i.e., $I(t) \sim 10^9$ A/sec) as the primary energy source. This is discharged into an intermediary storage inductor which in turn, serves as the means for the rapid transfer of energy to the detonation wave. Each loop is examined and characterized independently with the intention of optimizing the magnetic energy transfer to the resistive load shown in figure 1(b). A preliminary examination of LC storage circuit (figure 1(a)) is made by comparing an actual current "ring-out" against a set of computer generated derating curves to assess the extent of parasitic components. Analysis is then made on the LR discharge circuit under the assumption of rapid switch commutation.

---

[21] Korol'kov, V. L., Mel'nikov, M. A., and Tsyplenko, A. P., "Dielectric Breakdown of Detonation Products," Sov. Phys. Tech. Phys., Vol. 19, No. 12, p. 1569, June 1975.

[22] Datsenko, V. A., Korol'kov, V. L., Krasnov, I. L., and Mel'nikov, M. A., "Dielectric Breakdown of Detonation Products," Sov. Phys., Tech. Phys., 23 (1) p. 33, Jan 1978.

*RDX has relatively the same carbon product concentration as PBX 9404.

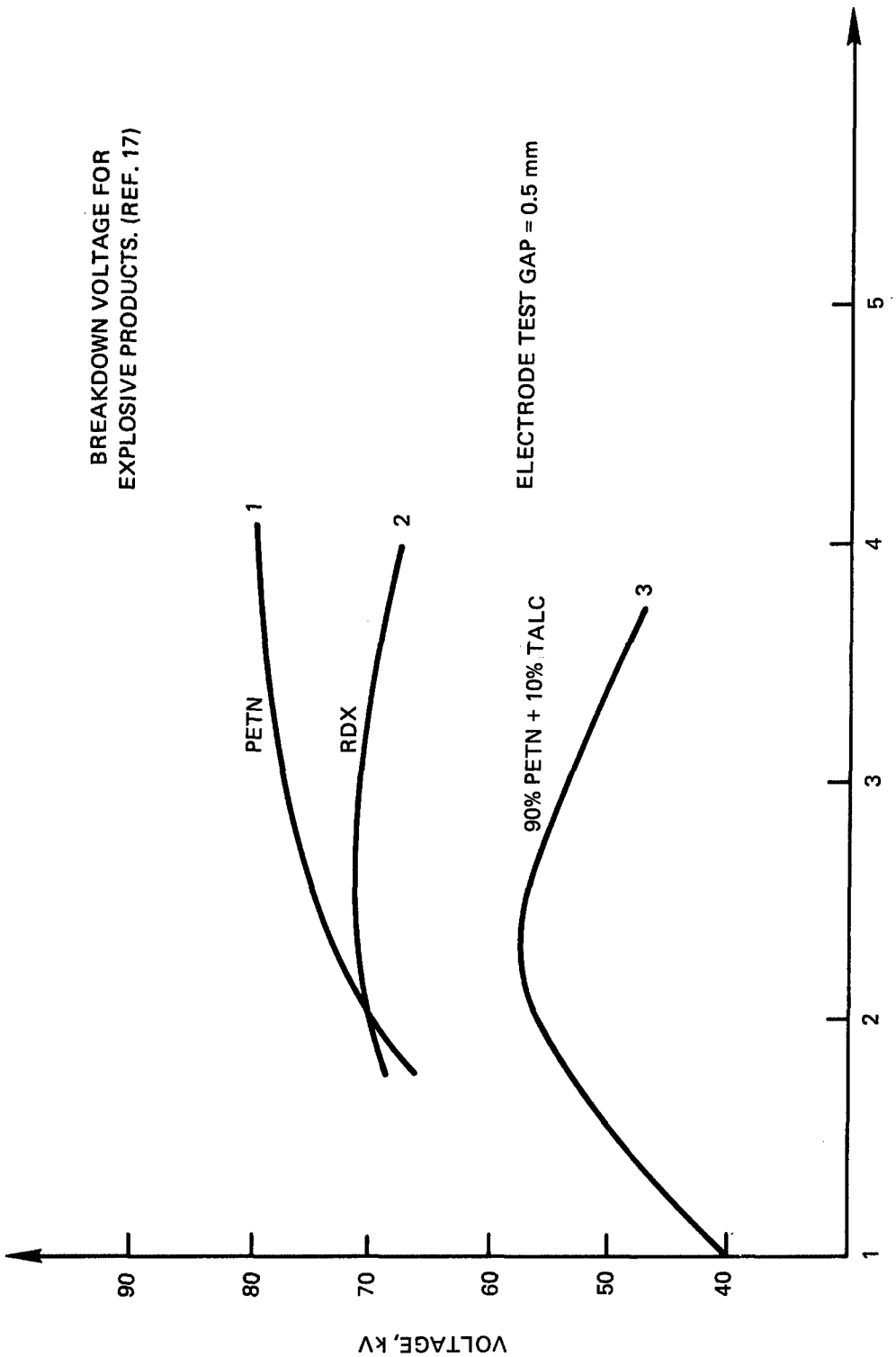

FIGURE 3 EXPERIMENTALLY DETERMINED DIELECTRIC STRENGTH IN THE PRODUCT ZONE FOR PETN, RDX AND 90% PETN, AS A FUNCTION OF TIME RELATIVE TO THE SHOCK FRONT

Ideal LC Network. On defining the ratio of the surge impedance to the loss resistance R by a dimensionaless parameter λ, where

$$\lim_{R\to 0} \lambda \equiv \lim_{R\to 0} \frac{1}{R}\sqrt{\frac{C}{L}} \to \infty \qquad (21)$$

is imposed in the limiting situation of negligible damping, the natural current response is characterized by a symmetrical, unattenuated sinusoid with its frequency typically given by

$$\omega \equiv 2\pi f = \left[(L_j + nL_s)C\right]^{-1/2} \quad \text{(Hz)}. \qquad (22)$$

The inductance in this instance accounts for stray component inductances L_j as well as for the storage inductor L_s. Specifically if n defines the number of bank capacitors, each of capacitance C, with component dissipation assumed negligible and generally, with $L_s >> L_j$, Equation (22) expresses the characteristic natural frequency of the LC circuit. $V_c(0)$ equals the initial charging voltage across the capacitor bank. For 5 kV across the paralleled arrangement of thirty six 240 microfarad (15 nH) capacitors, the quarter-period pulse should (ideally) energize a 7.4 microhenry inductive load to a peak energy of 108 kilojoules in 397 microseconds. Neglecting the various dissipative losses, the undamped peak current condition responsible for the magnetic flux energy stored in the inductor is simply

$$i_{max} = V_c(nC/L_s)^{1/2} \qquad (23)$$
$$= 170 \text{ kiloamperes}$$

In actual "best case" situations, various dissapative mechanisms generally reduce this value by about 20%. The rate of energy transfer to the inductor depends only on the initial value of the current derivative; the rate of current rise in the inductor in this instance is

$$\frac{d}{dt}(ni)\Big|_{t=0} = V_c(0)/L_s \qquad (24)$$

or,

$$\sim 0.7 \text{ gigamperes/second}$$

LCR Network for the Capacitor-to-Inductor Loop. Figure 4a represents an example of the diminuted (current) output from the bank "rang down" through the 7.4 microhenry inductor. This measured response will be compared against the damping curves in Figure 4b to provide a realistic means to access the nature of the observed current suppression accrued by the circuit.[23] In this particular

[23] Greenwood, A., Lee, T. H., "Generalized Damping Cruves and Their Use in Solving Power-Switching Transients," Trans, IEEE, Vol. 82, Part III, p. 527, 1963.

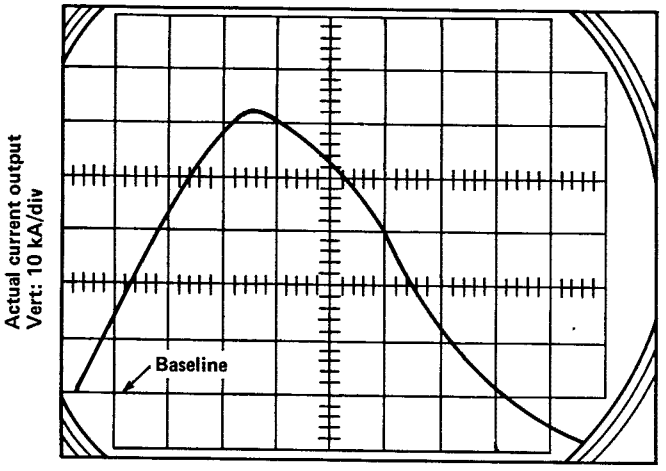

(a) Actual bank LRC current pulse profile, before line trimming. Ultimately, 24% increase in the peak, at 394 μ sec, resulted from trimming .

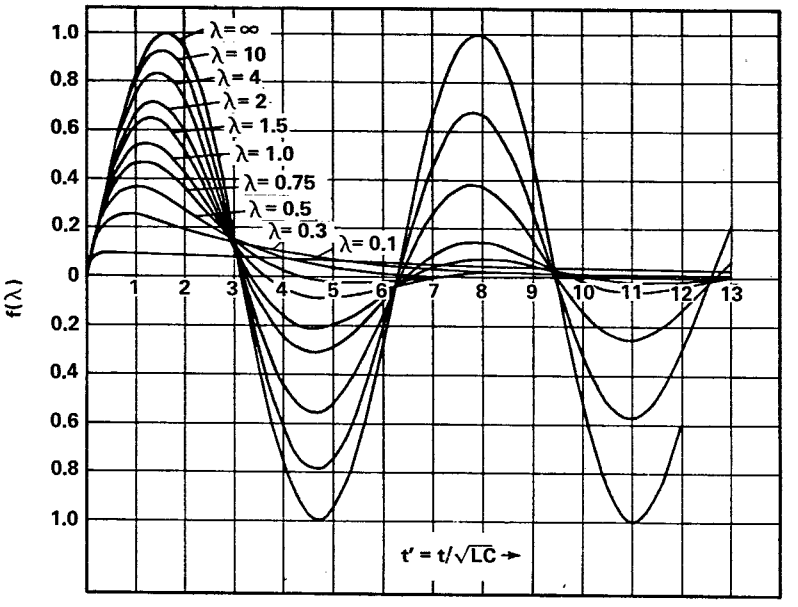

(b) Generalized plot of inverse transform, generated by equation (35), (Ref. 23). This illustrates the derating of the capacitor inductor network due to stray component inductances and resistances

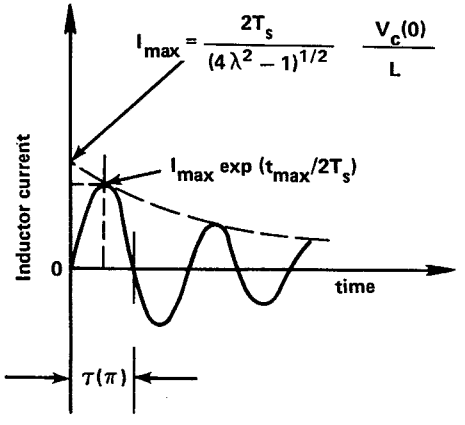

(c) Illustrating the terms used in equations (35) and (39) for the inductor current in an underdamped series LRC circuit; $\lambda > 0.5$

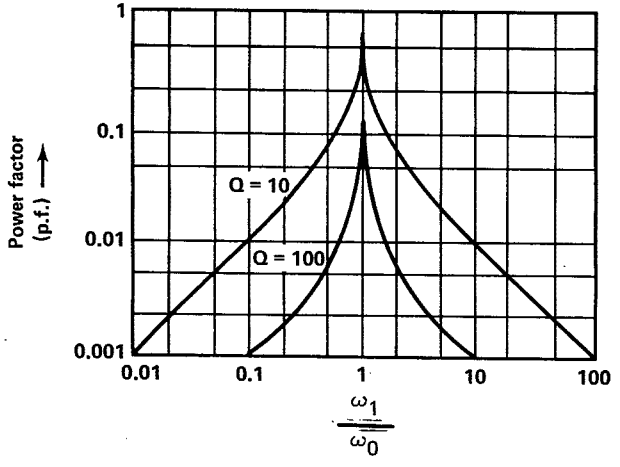

(d) The power factor curve illustrating the extent of parasitic losses to LC circuit components — as determined by equation (46)

FIGURE 4 OBSERVATIONS OF THE SERIES RLC CIRCUIT DISSIPATIVE BEHAVIOR

instance pulse derating is significantly evident in both the amplitude suppression and the premature quarter-period peak; the quarter-wave misphasing compounds the problem subsequently resulting in abnormal switching conditions incurred through switch mis-timing. Once characterization and adjustment for such losses is made, independent consideration can be given over to the capacitive switching problems, specifically disconnecting the capacitor bank from the storage inductor.

A preliminary analysis of circuit conditions in the capacitor-to-inductor loop, including various circuit switching components, indicates that this more involved network can ultimately be reduced to an elementary LCR network. The circuits response is generally described by the second order equation

$$R \frac{d^2}{dt^2} I(t) + L \frac{dI}{dt} + \frac{I}{C} = 0 \quad , \tag{25}$$

or

$$\frac{d^2}{dt^2} I(t) + \frac{1}{T_s} \frac{d}{dt} I(t) + \frac{1}{T^2} I(t) = 0 \quad . \tag{26}$$

The coefficients T_s and T^2 designating the characteristic time constants are defined by

$$T_s = L/R \ , \ T_p = RC \ ; \tag{27}$$

inverted, their product

$$T^2 = (L/R)(RC) = LC \quad , \tag{28}$$

emerges as the so-called natural frequency given by Equation (22) where

$$\omega_o \equiv (LC)^{-1/2} = 2\pi f \ . \tag{29}$$

Also, the quotient expression gives

$$\frac{T_s}{T_p} = \frac{Z_o^2}{R^2} \equiv \lambda^2 \quad ,$$

to again regain the condition given by expression (21) where

R ≡ the equivalent network loss resistance,

C ≡ the total bank capacity (including stray capacitance),

$L \equiv$ the lumped inductances of the circuit loop

$Z_o \equiv$ the surge impedence $\sqrt{L/C}$ (ohms).

The current response is subsequently specified by defining the capacitor charging voltage $V_C(0)$ and is generally expressed in terms of the (instantaneous) potential driving a load with impedance Z:

$$I(t) = Z^{-1} V(t) \quad . \tag{30}$$

Operational solutions to Equation (26) are conventionally expressed by the inverse Laplace transform response of[23]

$$i(s) = \frac{V_C(0)}{L} \frac{1}{s^2 + \frac{s}{T_s} + \frac{1}{T^2}} \quad . \tag{31}$$

For the case where underdamped conditions prevail such that

$$R < 2Z_o \ , \ \lambda > 0.5 \ ,$$

we have that

$$I(t) = \frac{V_C(0)}{L} \frac{2\ T_s}{(4\lambda^2-1)^{1/2}} \exp\left(\frac{-t}{2T_s}\right) \sin\left((4\lambda^2-1)^{1/2}\ t/2T_s\right). \tag{32}$$

As the various component resistances diminish this equation again reduces to the idealized limit of a simple LC circuit typically given by

$$I_{\text{undamped}} = \frac{V_C(0)}{Z_o} \sin \omega_o t. \tag{33}$$

Defining the dimensionless parameter t' by

$$t' = t/\sqrt{LC} \ , \tag{34}$$

and using the undamped LC case, Equation (33), as the standard for comparison, Equation (32) reduces to

$$\frac{I(t')}{V_C(0)/Z_o} = \frac{2\lambda}{(4\lambda^2-1)^{1/2}} \exp\left(\frac{-t'}{2\lambda}\right) \sin(4\lambda^2-1)^{1/2}\ t'/2\lambda \ . \tag{35}$$

The family of curves in Figure 4b are generated from this.[23] The utility of such curves is seen in analyzing the situation depicted by Figure 4a. The moment the charged bank is switched, the ensuing current is limited by the surge impedance of the network loop comprising the bank-to-inductor circuit and their interconnections. Component inductances are not, a priori, assumed negligible, and the inherent circuit resistance further suppresses the inrush current response. Observable effects from stray capacitance (such as that between adjacent coil turns of L_s) are determined to be relatively negligible in this instance. The most severe condition is considered when the voltage is at its peak at the time of switching. To assess the loop inductance, two conditions on the first half-cycle current waveform are noted. Setting the first time derivative of Equation (32) to zero gives the following relation

$$\tan \frac{(4\lambda^2-1)^{1/2}}{2T_s} t\Big|_{t_{max}} = (4\lambda^2-1)^{1/2} . \qquad (36)$$

Evaluated at the first extreme $t \equiv t_{max}$, this expression gives the characteristic time constant T_s. On defining

$$\omega_1 \equiv \frac{(4\lambda^2-1)^{1/2}}{2T_s} , \qquad (37)$$

Equation (36) is simply recast as

$$T_s = \frac{0.5}{\omega_1} \tan (\omega_1 t_{max}) . \qquad (38)$$

Also, observing that the first crossover point of the waveform ($\tau(\pi)$ in Figure 4c) occurs at time

$$\frac{2T_s}{(4\lambda^2-1)^{1/2}} \pi = \frac{\pi}{\omega_1} , \qquad (39)$$

makes Equation (38) fully determinable. In the particular instance (from Figure 4a)

$$\tau(\pi) = \frac{\pi}{\omega_1} = 800 \text{ microseconds},$$

$$t_{max} = 350 \text{ microseconds},$$

and we have

$$T_s = \frac{(0.5)\,(8\times10^{-4})}{\pi} \tan\left[\frac{(3.5\times10^{-4})\pi}{8\times10^{-4}}\right],$$

or

$$T_s = 640 \text{ microseconds.}$$

The circuit's loop inductance can then be obtained directly by noting the onset of the exponential envelope (i.e., "ultimate" peak current) is specified by the relation (Figure 4c)

$$\left(\frac{2T_s}{(4\lambda^2-1)^{1/2}}\right)\left(\frac{V_c(0)}{L}\right) = \frac{\tau(\pi)}{\pi}\left(\frac{V_c(0)}{L}\right), \qquad (40)$$

The observed first peak current is given by

$$I_{obs} = I_{max} \exp\left(\frac{t_{max}}{2T_s}\right) = \frac{\tau(\pi)}{\pi}\left(\frac{V_c(0)}{L}\right) \exp\left(\frac{t_{max}}{2T_s}\right) \qquad (41)$$

The realistic network inductance is then given in terms of the (current) waveform trace and known circuit parameters

$$L = \bar{\tau}(\pi)\left(\frac{V_c(0)}{I_{obs}}\right) \exp\left(\frac{t_{max}}{2T_s}\right), \qquad (42)$$

with $\bar{\tau}(\pi) \equiv \tau(\pi)/\pi$.

For $V_c(0) = 2.8$ kilovolts,

$I_{obs} = 53.8$ kiloamperes,

$t_{max} = 350$ microseconds,

and $T_s = 640$ microseconds.

The circuit loop inductance is 17.4 microhenries; subsequently stray and component inductances are particularly significant in this case. Equation (23) for peak current with no damping gives

$$\frac{V_c(0)}{Z_o} = V_c(0)\sqrt{\frac{nc_n}{L}} = 2{,}800\sqrt{\frac{(36)\,(240)}{17.4}} = 62{,}392 \text{ amperes peak}$$

To effect the peak current portrayed by the current waveform (in Figure 4a), a per unit current reduction of 53.8/62.4 = .86 must occur. Referring to Figure 4b indicates that $\lambda = 7$ satisfies our conditions. With the surge impedance $Z_o = 45$ milliohms, the loop loss resistance as given by

$$R = Z_o/\lambda \quad , \qquad (43)$$
$$\simeq 6.4 \text{ m}\Omega$$

This is the resistance limiting the current to 53,800 amperes in the capacitor-to-inductor loop otherwise approaching 55,748 amperes.

The instantaneous power transferred is resolved into active (i.e., dissapative or energy absorbing) and reactive (i.e., energy-storing) components; the respective phase factors are the power factor and the reactive factor.

Addressing for the moment only the dissapative component, the time average power dissipated to the circuit during the first quarter-period is typically

$$\langle P \rangle = \frac{1}{t_{max}} \int_0^{t_{max}} I(t) V_c(t) dt \; . \qquad (44)$$

From this the "effective power" is given by

$$P = \frac{|I(t)|_{max}}{t_{max}} \; V_c(0) \; x \; (p.f.) \quad . \qquad (45)$$

The extent of power dissipation in the circuit during the inductor energizing phase can be illustrated by the power factor (p.f.). A low dissipation factor is a good criterion for the circuit performance here. For a series, inductor dominated, LCR circuit the (lag) power factor is given by

$$(p.f.) = \frac{R}{|Z|} = \frac{R}{\left[R^2 + (\omega_1 L - \frac{1}{\omega_1 C})^2\right]^{\frac{1}{2}}} \qquad (46)$$

(the active component phase factor between the instanteous current and the instantaneous voltage)

where $L = L_s + \sum_j L_j$

As (p.f.) decreases, progressively greater currents are delivered to the inductor L_s. The ratio of the maximum energy stored to the energy loss in a given power pulse, conventionally referred to as the quality factor (Q) for the circuit, is a directly measurable quantity that indicates the extent of damping and time misphasing. For a series LCR circuit this is generally defined as

$$Q \equiv \omega_o L/R = \frac{1}{R}\sqrt{\frac{L}{C}} \quad . \tag{47}$$

Consequently, the reactive factor Q (or equivalently, λ) can be used to explicitly determine the amount of stray inductance L_j, and hence accurately determines the extent of misphasing in the circuit. With

$$R = \frac{1}{Q}\sqrt{\frac{L}{C}} \quad \text{and} \quad \omega_o = \sqrt{\frac{1}{LC}} \quad \text{then}$$

$$\omega_1 L - \frac{1}{\omega_1 C} = Q\,\frac{\omega_1}{\omega_o}\left(1 - \frac{\omega_o}{\omega_1}\right) \tag{48}$$

Equation (46) results in

$$(p.f.) = \left[1 + Q^2\left(\frac{\omega_1}{\omega_o}\right)^2 \left(1 - \frac{\omega_o^2}{\omega_1^2}\right)^2\right]^{-\frac{1}{2}} \tag{49}$$

Figure 4d illustrates the generalized family of power factor curves that one can typically generate directly from equation (49) with the characteristic parameter being Q. As a rather dramatic example of power lost, initially where 53.8 kiloamperes is transferred under "lossy" conditions: $\lambda = 7$; p.f. = 0.4. From Equation (45) the "effective power" pulse dissipated is .17 gigawatts or about 40% of the total available power pulse.

For systems with large Q and λ, $\omega_1 \simeq \omega_o$ as Figures 4b and 4d indicate the time misphasing diminishes and effective power comes principally from the reactive (i.e., the energy storage) component of instantaneous power. The optimum condition for the LR circuit is to have a high Q and a low power factor. This optimum condition can be approached in the present facility by using circuit lines with the lowest practical resistance and length.

LR Discharge Network. Current-detonation interaction commences with the disengagement of the capacitor bank and switching assembly. About 5 microseconds prior to the opening switch disruption the HE detonation event is initiated, thus effectively establishing the closed LR-discharge configuration. From this point the conductive channel of the reacting explosive serves to complete the current path across the explosive-electrode pair. By a proper adjustment of the storage inductor to match the characteristic resistance of

this conductive channel the resulting ratio of (R/L_s) uniquely prescribes the decay rate of the inductively stored energy in L_s and the subsequent rate of energy dissipation to the detonation wave.

The current response from a series LR discharge circuit is typically described by the circuit impedance $Z = R - i\omega L_s$. Figure 5 illustrates the current transfer to the conduction zone of the detonation wave for a set of detonation conductivities ranging from 0.4 to 4.0 mho/cm. L_s is the experimentally adjustable parameter required to match a given resistance. At this point of events the capacitor bank has been decoupled from the network (see Figure 1a, b). The case illustrated in Figure 5 uses a storage inductive value of 7.4 microhenries. Any decrease of magnetic field energy from the storage inductor must ultimately show up as dissipated energy in the resistive components of the circuit. Consequently the energy predominately goes into the conduction zone of the detonation wave as joule heat, i.e., $\eta(\xi)j^2$ (c.f. equation 8). On commencement of the detonation (designated as a time τ_D) the current response is described by conservation of energy as

$$-\frac{d}{dt}\left[\frac{L_s I^2(\xi, t)}{2}\right] = I^2(\xi,t)R(\xi), \text{ for } t \geq \tau_D. \qquad (50)$$

or

$$L_s \frac{dI}{dt} + IR = 0. \qquad (51)$$

with the definition $\gamma \equiv \frac{R(\xi)}{L_s}$ Equation (51) reduces to the simple linear homogeneous D.E.

$$\left[\frac{d}{dt} + \gamma(\xi)\right] I(\xi,t) = 0, \qquad (52)$$

where the explosive's resistance is $R(\xi)$.

Explicitly noting that the current transferred through the conduction zone is position dependent reiterates the fact conveyed earlier that the conduction zone is a nonisotropic, resistive fluid with exponentially increasing resistivity in the product region. This position dependence of conductivity is not used in the general treatment presented in this report. However, to treat the details of energy released in the reaction zone and how this energy is communicated to the detonation front will require knowing this spatial relationship of conductivity.

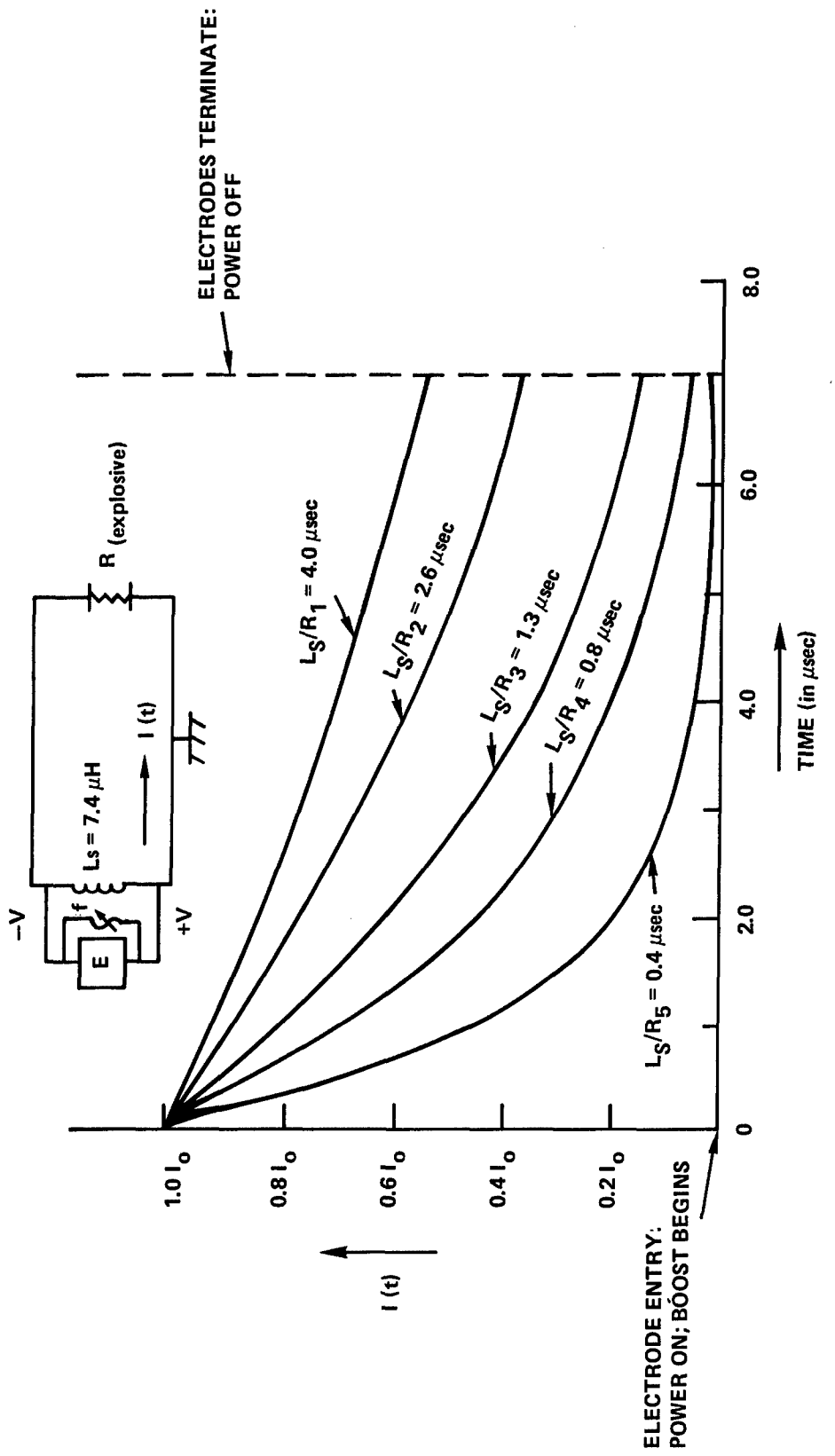

FIGURE 5 THE IDEALIZED CURRENT TRANSFERRED FROM THE STORAGE INDUCTOR TO THE CONDUCTION ZONE OF THE DETONATION WAVE. FOR VARIOUS EXPLOSIVE CONDUCTIVITIES, RANGING FROM 0.4 TO 4.0 mho/cm., L_s IS THE EXPERIMENTALLY ADJUSTABLE PARAMETER. THE CAPACITOR BANK HAS BEEN DECOUPLED FROM THE NETWORK.

Equation (52) can, of course, be directly integrated, and on employing the initial condition $I(\tau_D) \equiv I_o$ we get the familiar exponential decay of I_o in the storage inductor with time:

$$I(\xi,t) = I_o\, e^{-\gamma(\xi)t}, \text{ for } t>\tau_D, \text{ with the decrement} \quad (53)$$

being

$$\gamma \equiv \frac{R(\xi)}{L_s}, \text{ if } L_s >> \sum_j L_j \ . \quad (54)$$

The natural current response is specified by Equation (53) for times $t >> t_o$ and implies infinitely-fast switching. In actual practice, however, the current is driven by the (~2 μs) voltage spike generated during fuse rupture. The forcing function superimposes an additional "particular" solution. Consequently, in the time domain, the switching surge produces a "forced" response which is given by

$$I(t) = \frac{V_o\left[1-\exp\left(-Rt(L_j+L_s)/L_jL_s\right)\right]}{R\left[1 + (1/L_s)^2 L_j^2 L_s/(L_j+L_s)\right]^{\frac{1}{2}}} \exp(-\gamma t) \quad (55)$$

Under the assumption that the fuse-assembly inductance, $L_j << L_s$, Equation (55) reduces to the abbreviated form given by Equation (53). The particular scheme used here thus selects out the peak current $I(\tau_D) \equiv I_o$ excited at the frequency γ which represents the natural response if L_s is properly adjusted to the resistance of a specific explosive. This establishes the value for γ which corresponds to the transit time through the electrodes - the latter being preselected on the basis of the β-criteria established earlier by Equation (1.1). The current response for a typical range of (low current) explosive resistances in the time domain Equation (53) is shown in Figure 5.

Dissipative Power Available to the Explosive. Under actual power transfer conditions, the power absorbed by the modular opening switch unit itself must be accounted for. Some additional loss to vaporization of the exploding fuze (see circuit in Figure 5) also depletes a fraction of the available commutated energy at a rate

$$W_o = \frac{d}{dt}\ \frac{(LI^2)}{2} \ . \quad (56)$$

The remaining power available to the explosive detonation wave, on being driven by the circuit breaking unit's voltage is

$$W = IV - W_o \quad (57)$$

$$\simeq 10 \text{ gigawatts.} \quad (58)$$

Wo is the power loss to the circuit breaking unit.

If stray inductance effects and switch losses are assumed relatively negligible compared to L_s and the detonation wave resistance, the voltage for the LR-discharge circuit being driven by the (parallel) switching unit is inferred (under quasi-static conditions[20]) as

$$V = IZ' \tag{59}$$

where the real part of Z is Z' and the imaginary part is Z'', i.e.,

$$Z = Z' + iZ'' \tag{60}$$

The expression for Z can be regarded as representing the first terms in an expansion of the functions $Z(\gamma)$ in powers of the frequency. The first term Z' represents a pure resistance, hence direct ohmic heating. The effect due to the second term Z'', arises because the magnetic field induced by a variable current in the electrodes generates eddy currents and therefore an additional dissipation of energy in the detonation.[20,24] This "induced" ohmic effect is discussed on page 17 from a different viewpoint and detailed in Appendix A.

The joule heating (i.e., the power dissipated) in the detonation wave conduction zone is purely D.C. ohmic in nature and is thus simply given by

$$I^2Z' = I^2R(\xi)$$

where $R(\xi)$ is the conduction zone resistance. I is the current transferred through that resistance when driven by the non-linear EMF generated by the exploding wire fuse. Within the particular idealized experimental limitations considered here (eg. no switch losses, etc.) the maximum rate of energy transfer from the 7.4 μH storage inductor is V/L_s = 13.5 GW of power driven into the explosive load.

For a L_s/R of 0.4μsec (See Figure 5) and a postulated transfer of 170 kA, the maximum energy transfer to the explosive's detonation wave is found by integrating the instantaneous power expression over time. This results in

$$U = \frac{L_s I_o^2}{2} \left[\exp\left(-2 \frac{R}{L_s} \tau_D\right) \right] \tag{61}$$

$$\approx 107 \text{ kilojoules}$$

[24] Chu, B. T., "Thermodynamics of Electrically Conducting Fluids," Physics of Fluids, Vol. 2, No. 5, p. 473, Oct 1959.

For a 10 gm explosive sample with approximately 5 kJ/g detonation energy density, there could be as much as a factor of 2.2 increase in observed enhancement of energy for the present experimental arrangement.

As calculated in Appendix A, for the particular coaxial accelerator geometry and explosive resistivities considered here, the 101 J incurred through magnetic diffusion is insignificant compared to the direct-contact ohmic heating effect of Equation 61. Under properly parameterized conditions the contribution to deposited energy by the magnetic diffusion process can be large. This subject will be addressed in future work.

A DESCRIPTION OF THE EXPERIMENTAL ARRANGEMENT USING A FIXED CAPACITIVE ENERGY

The actual experimental facility is shown in Figure 6. It was schematically depicted in Figure 1 as a two loop network comprised of the bank array, the storage inductor, the resistive load (i.e., the reacting explosive), and various switching assemblies. In actual practice these circuits entail a number of surge components comprising a variety of dissipative and transient effects. A scheme employing a set of generalized damping curves is used to characterize the LC loop (shown in Figure 1a) under actual network loading conditions.

The capacitor bank currently in use consists of nine modules, each containing four, 240 microfarad (5 kV) capacitor units. The bank array is configured in a parallel arrangement to deliver optimal current to a 7.4 microhenry inductive load during the first quarter period of a 630 hertz, underdamped oscillation. Ideally, the waveform is truncated at the first current maximum to achieve optimal energy density at the inductor. This is accomplished by rapidly interrupting the capacitor-to-inductor circuit at that instant - the generated emf across the inductor going into driving the current through the resistive (explosive) load hence transferring the stored magnetic energy to the detonation wave.

Direct coupling from the slow bank to a highly resistive explosive produces an unfavorably long pulse, subsequently imparting only a small fraction of the available capacitive energy into the detonation. The nominal resistive load values typically characteristic of the dense detonation processes envisioned here indicate that it is not possible to increase the RC-time constant much above a few milliseconds. However, satisfying Equation (1) requires that the detonation front transit through the electrode pair in about 10 microseconds - the current pulse thus lags by about two orders of magnitude. To circumvent this problem the low impedence storage inductor is inserted in parallel between the bank and the electrode pair to serve as a fast response, intermediary current source.

The Use of Inductive Storage Schemes for Rapid Energy Transfer. Salge and Braunsberger have discussed the use of various inductive storage schemes to pulse shape the current output from

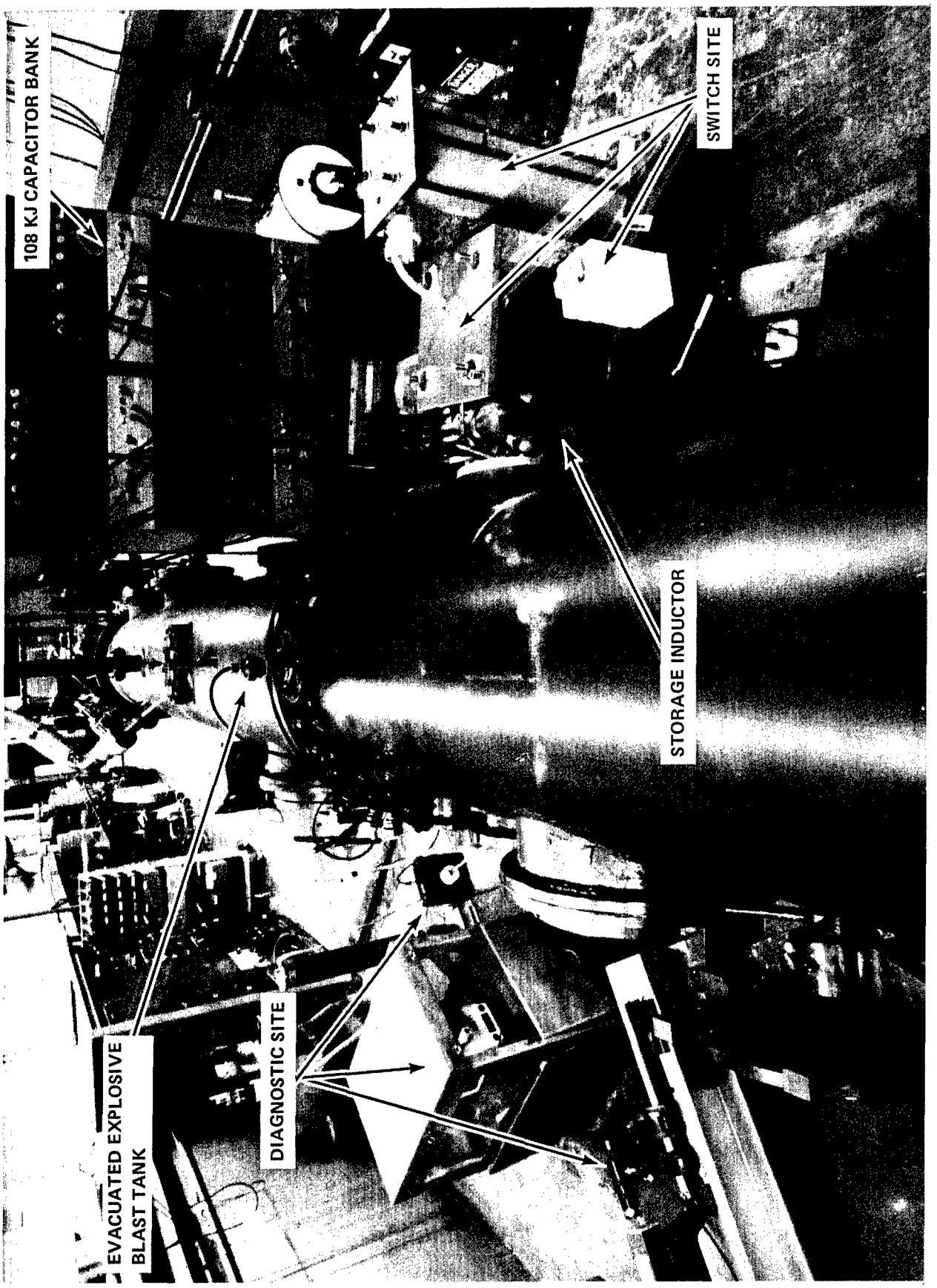

FIGURE 6 ACTUAL TEST FACILITY SETUP

large capacitor banks, specifically in applications related to high amplitude, microsecond current responses.[25] Once the mean, high current resistance of the detonation wave has been established an adjustable, bitter-type storage inductor can be employed to replace the existing 7.4 microhenry helical unit. This will provide the necessary versatility to tune the network inductance for optimizing the capacitor energy transfer to the resistive detonation wave.

During the course of designing this experiment, two helical solenoid designs were employed, both using high quality copper stock as the conductive element. The conversion of a high energy capacitor pulse of 0.17 MA generates an axial magnetic field near a quarter of a megagauss. Consequently, mechanical stress loads on the order of 246 MPa are realizable. The initial design given in Figure 7 consist of a 0.5 inch solid stock, 10-turn helical coil, internally constrained by a 4.5 inch diameter "Lexan" mandrel to check the inward radial over-stressing, and the compressive forces of the end turns. A highly dielectric elastomer separated the individual windings. The entire coil assembly was encapsulated by a one inch thick, epoxy - reinforced, fiber-glass boot. This construction is very bulky and lacks required versatility when changing the inductance value, i.e., by installing additional turns, or coils. The second design, the Bitter Disks type construction is also a single layer solenoid. However, instead of filamentary type windings, this design employs a set of copper disks; each turn is split radially and the split edge slightly displaced out of the disk planeto form a step which overlaps with the previous, adjacent disk. "The disks are interleaved with each other and with similar disks of insulation to form a continuous helix", as illustrated in Figure 8.[26] Clamping the desired number of disk stacks together provides a versatile and relatively compact storage inductor.

Component and Switching Assemblies.

ARRANGEMENT FOR SEQUENCING EVENTS. Figure 9 is a block diagram illustrating the various events as they typically occur in the actual experimental setup. Trigger information via a central control console (ITIG) enjoins three main-channel networks to properly coordinate the respective timing of the various firing line and switching assemblies. As depicted in Figure 9 (by the dashed network) a 357 microsecond delayed trigger pulse to the Explosive Initiation Network (EIN) evolves from this point. EIN enlists the use of two 10 kV pulsers, one of which initiates an exploding bridgewire detonator (E. B. W. DETR) which in turn initiates a 3 cm pentolite booster

[25] Salge, J., and Braunsberger, U., "Inductive Energy Storage Systems Applied for the Extension of Current Pulse-Duration of Capacitor Banks," Symp. Fusion Technology, 7th, Grenoble, Oct 1972.

[26] Frungel, F. B. A., High Speed Pulse Technology, Vol. 3, Academic Press, Inc., New York, p. 353, 1976.

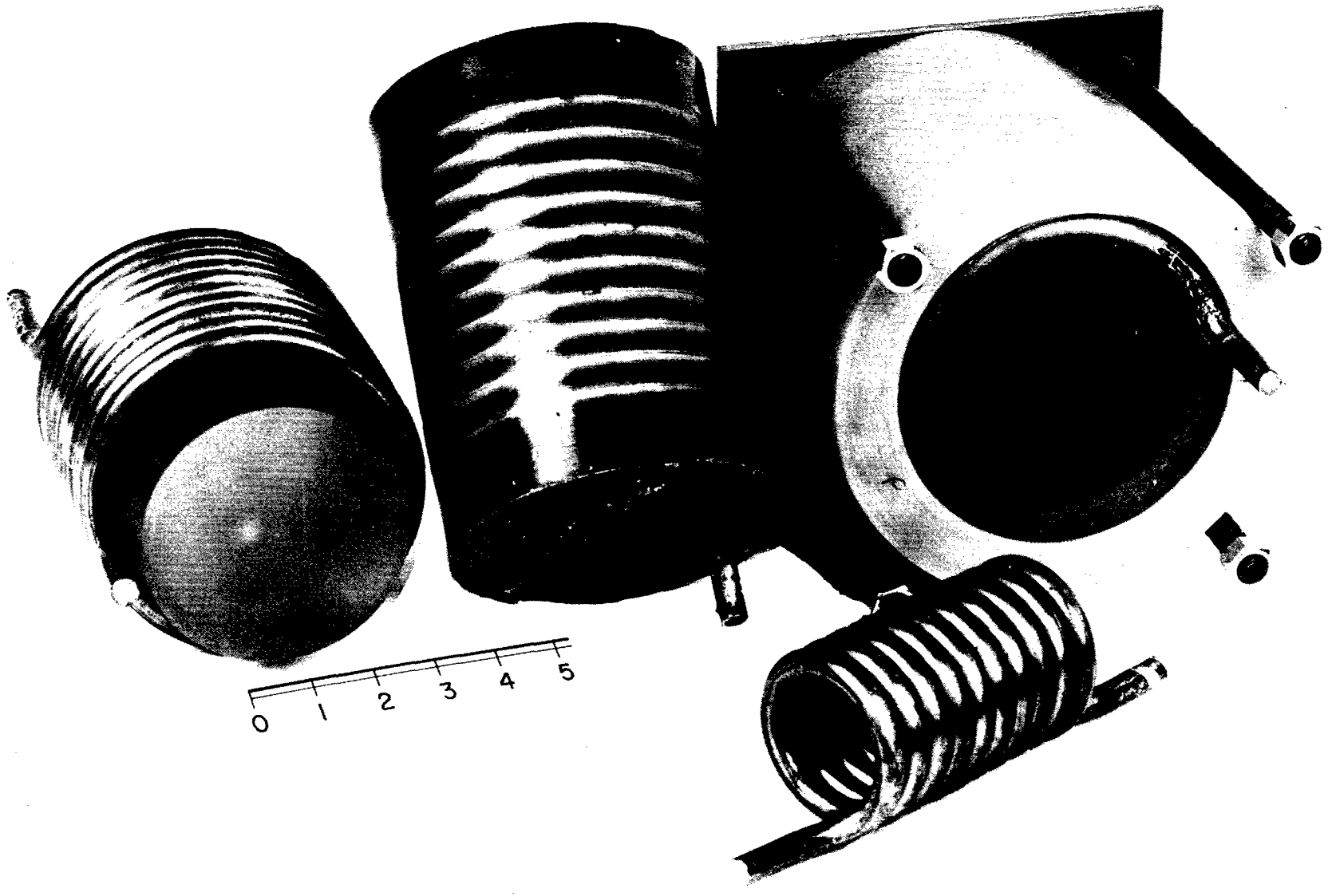

FIGURE 7 **ASSEMBLY COMPONENTS OF THE 1.0 AND 7.4 μH HELICAL STORAGE INDUCTORS.** Clockwise: 7.4 μH coil with "Lexan" Mandrel inserted; coil system shown encapsulated in a rigid, high-dielectric elastomer; assembly inserted in a tight fitting 1.5 inch thick, high tensile strength, fiberglass-epoxy composite shoe. Below the 7.4 μH assembly is a 1.0 μH, multi-turn coil unconstrained.

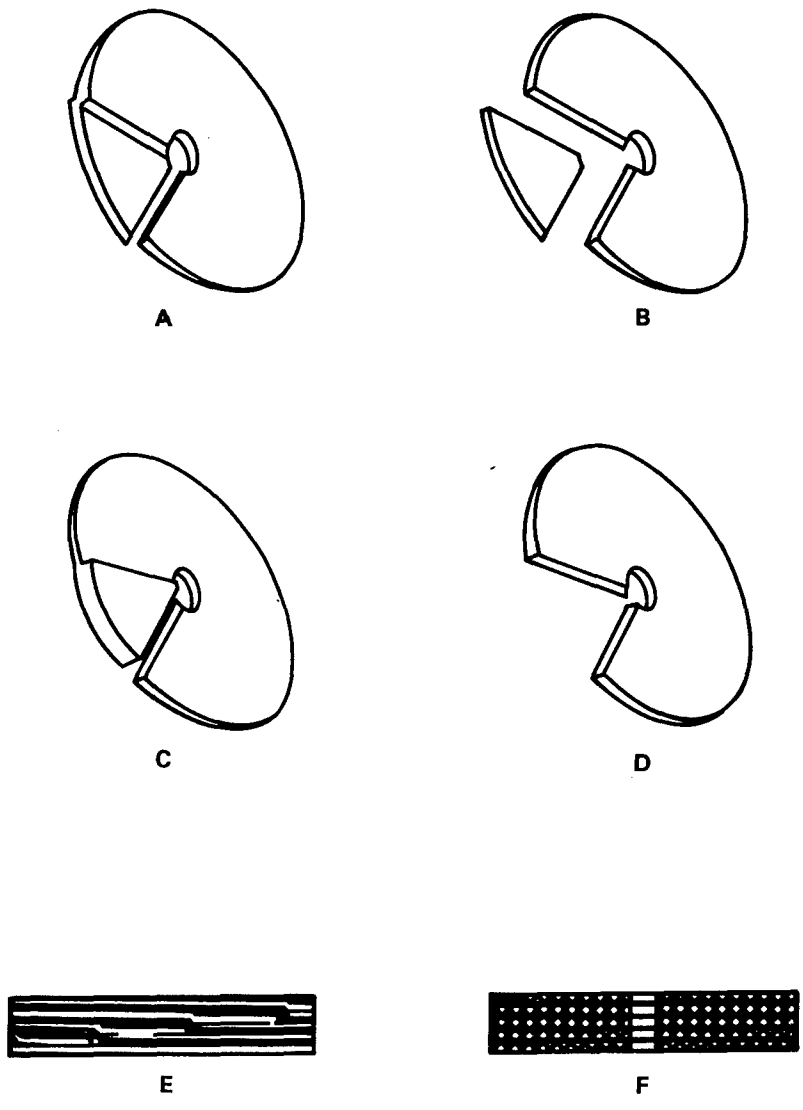

FIGURE 8 SCHEMATIC DIAGRAM DEPICTING COMPONENTS FOR A BITTER-TYPE, DISK INDUCTOR

Coil Components:

(A) stamped conductor disk with insulator disk (B)
(C) milled conductor disk with insulator disk (D)
(E) assembly, side view
(F) assembly, cross section

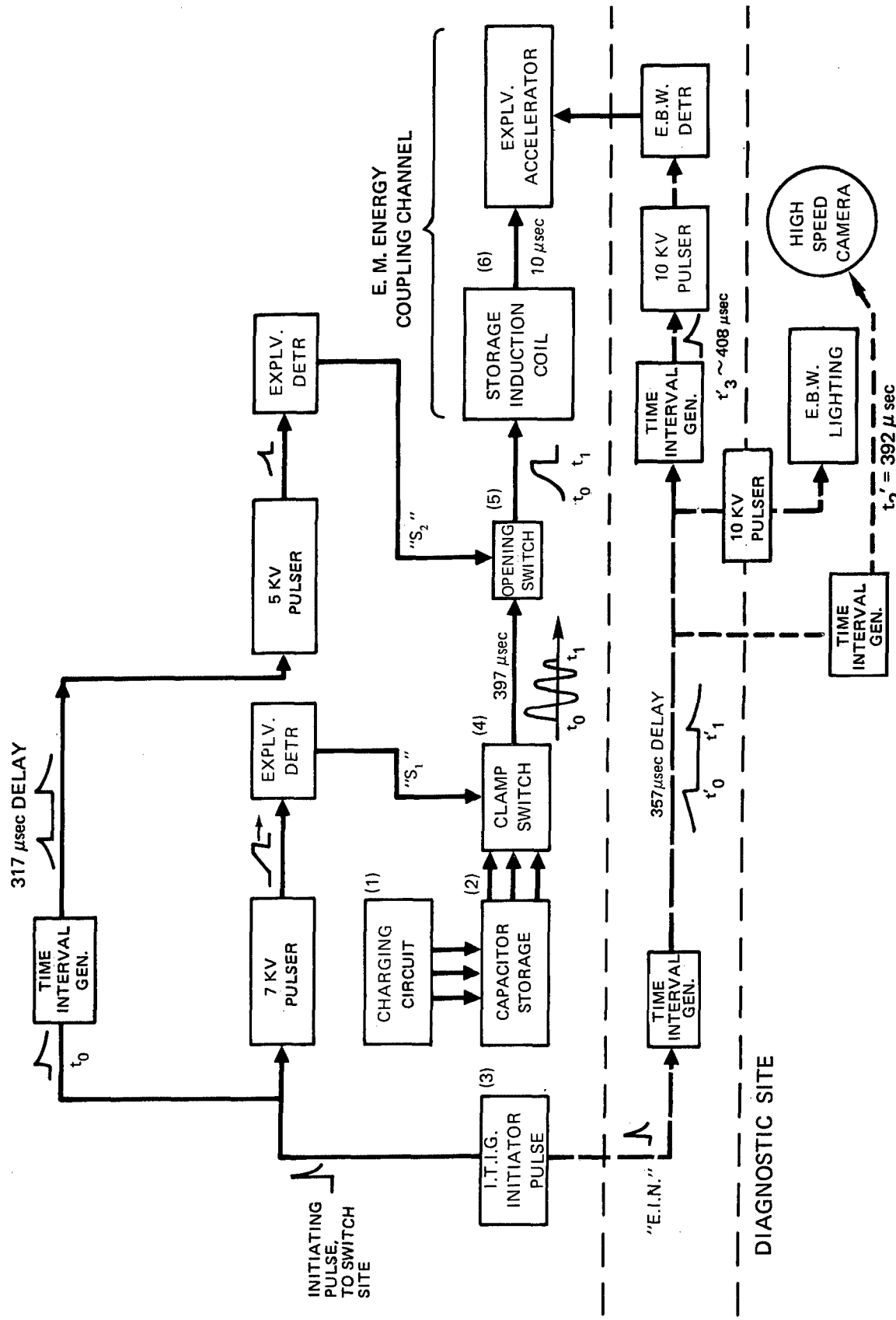

FIGURE 9 A BLOCK DIAGRAM ILLUSTRATING THE ELECTRONIC ARRANGEMENT FOR THE ACTUAL EVENT SEQUENCING.

interfacing the HE sample. The other unit 307 microseconds delayed, supplies a 10^3 7 kV pulse to a 3 cm (2 mil tungsten) exploding bridge-wire (EBW) light source. The 100 microsecond light pulse generated from this EBW provides an intense frontal illumination source for streak camera photography. The EIN is initially delayed 307 micro-seconds to allow adequate time for the electrical response of the opening switch. Terminating the EIN is 113 grams of explosive.

The second information channel initiates the S_1-trigger circuit. S_1 activates the switching assembly to clamp the capacitor bank on line once it is up to charge. A 7 kV transformer isolated pulser initiates three (EBW) detonators to explosively drive the clamp switch into closure. The enjoining circuit (in Figure 5) is further delayed 317 microseconds to allow for the current buildup in the storage inductor. Time-based from the clamp switch closure the trigger pulse S_2 is retarded 90 microseconds to allow the modular opening switch (MOS) the necessary induction time required for full mechanical response and a subsequent 40 microseconds to complete voltage recovery. Figure 10 depicts the idealized electrical responses in various circuits displayed in the correct timing sequence.

DESCRIPTION OF THE SWITCH ASSEMBLIES.[27,28] The switch assemblies currently employed are part of a developed tech-nology used in the Naval Research Laboratory's "Linus" fusion reactor program. Only a brief description of these are presented here. The capacitor bank is brought on line by rupturing a solid-dielectric insulator such as that employed by the switching arrangement illus-trated in Figure 11. The shutter mechanism for this switching unit enlists the use of a 217 mg explosive EBW detonator to mechanically drive a small section of aluminum channel plate through the dielectric stand-off (as illustrated in Figure 11a). The plate is connected to the low side of the bank circuit. Experiments using various thick-nesses of polyethylene indicate that the driven section channel (a 2-3 cm cylindrical boss) is capable of completing closure with about $\pm$ 0.5 microsecond jitter. To deliver the (5 kV) 170 kA current, three switch units are fired in parallel. On a trigger command these are simultaneously driven through the polyethylene dielectric and into a set of contact anvils (Figure 11b). The advantages of these solid-dielectric switches over other types of conventional closure devices are derived from the inherent simplicity of a unit with the capability of closing a circuit with a large, slow pulse and yet maintaining minimal shutter jitter, pulse distortion and negligible power loss. Using a 0.05 cm thick piece of polyethylene to hold off 5 kV the observed response time for three paralleled switch units is about 12.0 $\pm$ 0.5 microseconds.

---

[27] Ford, R. D., and Young, M. P., "Chemical Detonator Solid-Dielectric Switches for Starting and Clamp Applications," Proceedings of the 8th Symp. on Fusion Tech., EUR 5182e, Sep 1974.

[28] Ford, R. D., and Vithovitsky, I. M., "Explosively Activated 100 kA Opening Switch for High Voltage Application," NRL Report No. 3561, Jul 1977.

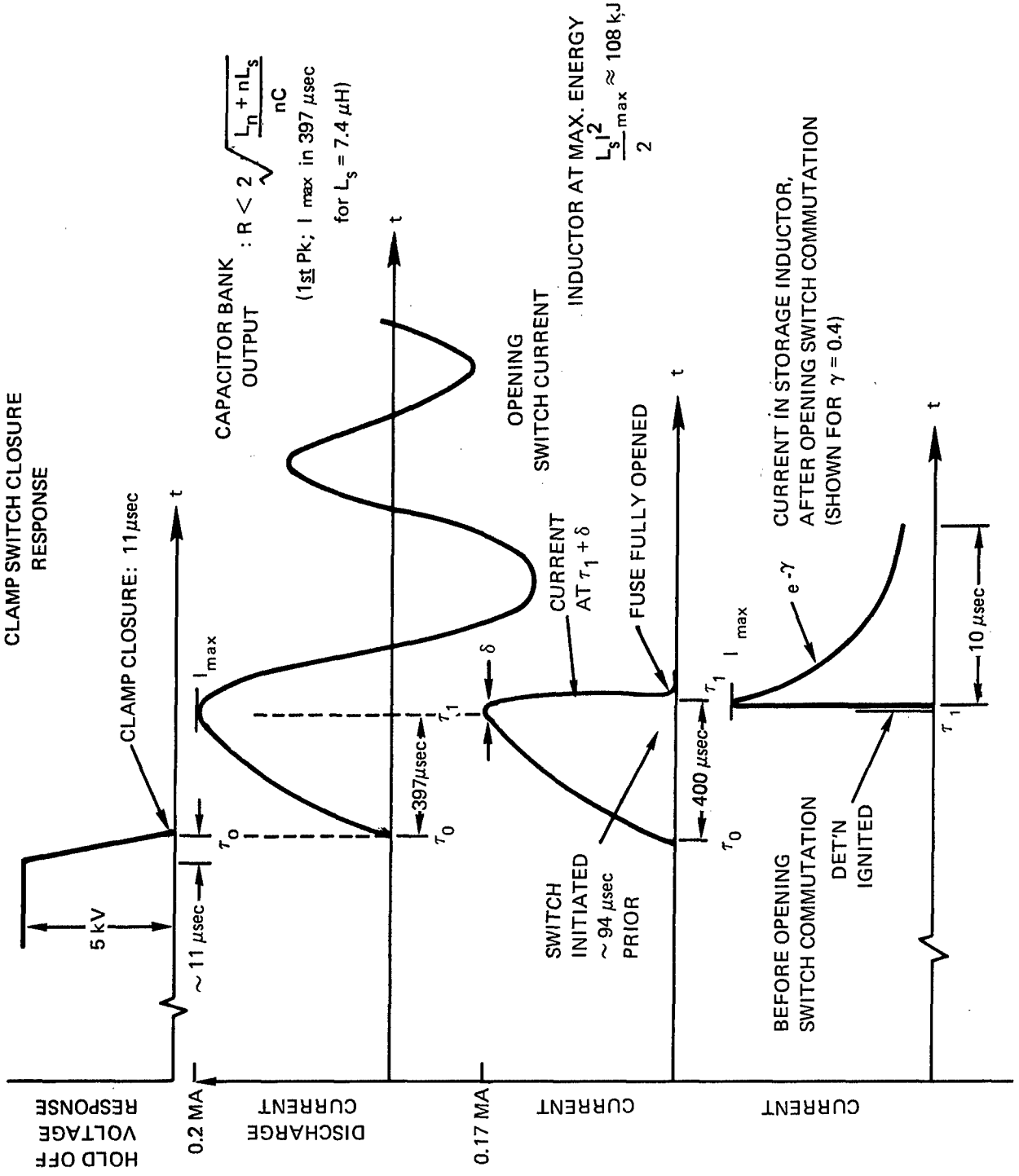

FIGURE 10 IDEALIZED SWITCH RESPONSE PROFILES: TIMING SEQUENCE OF EVENTS

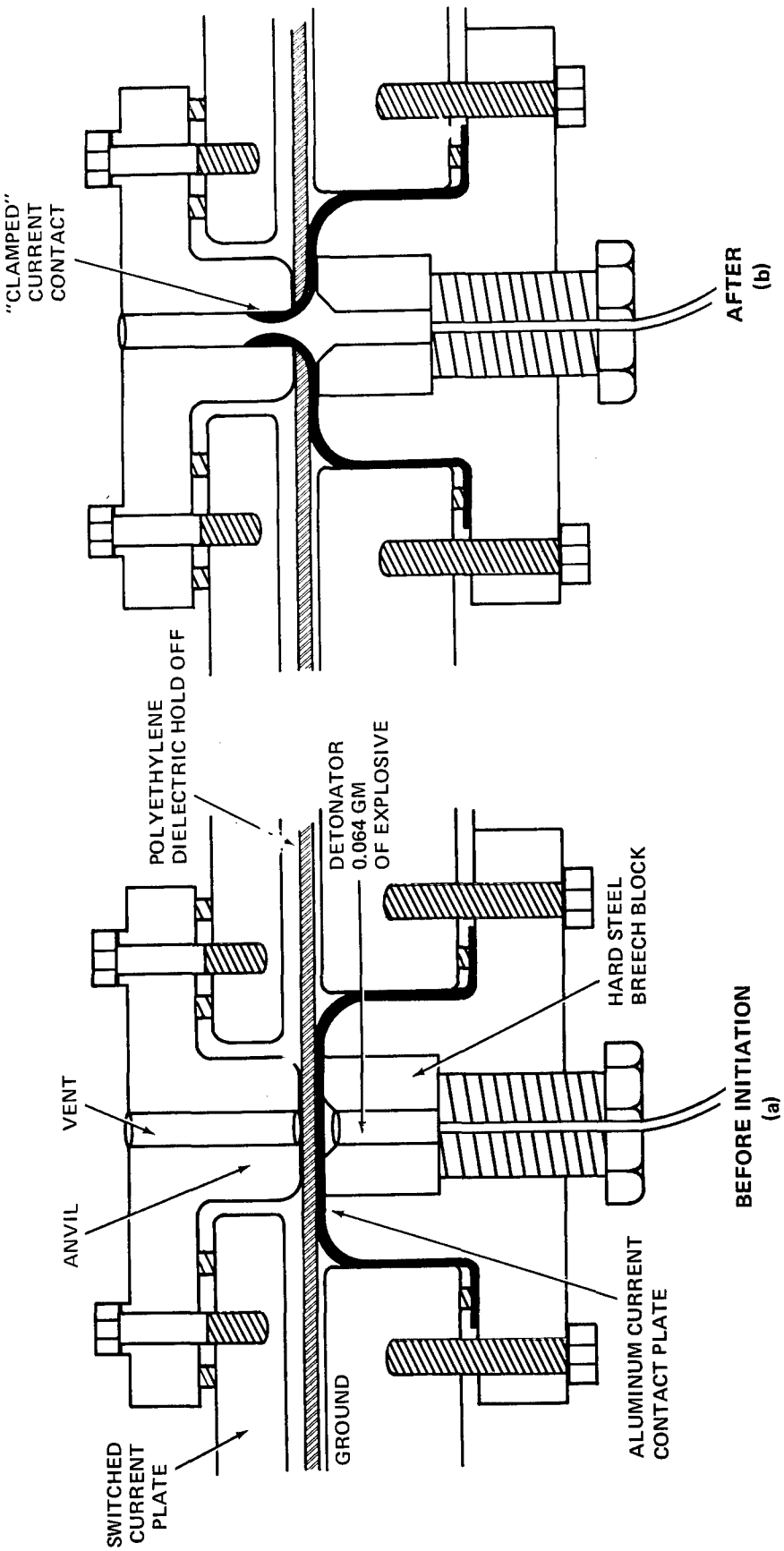

FIGURE 11 SOLID-DIELECTRIC CLAMP SWITCH USED IN CAPACITOR STARTING APPLICATION. (REF. 27)

The bank is disengaged from the circuit by mechanically severing the circuit loop. The opening switch shown in Figure 12 is a modular assembly designed to interrupt the current in the capicator-to-inductor loop at peak current. The particular breaker switch presently being used is an explosively activated, twelve stage switch capable of achieving the necessary electrical interruption in less than 40 microseconds. Parallelling a 60 cm filamentary exploding wire in a low inductance configuration with the switch provides the required current commutation rate for necessary voltage recover, consequently suppressing arcs and switch restrike to individual switch sections. Under optimal conditions the power consumption required to vaporize these copper wire fuses is expected to be relatively low - depending only on the mass and heat of vaporization of the copper. The use of aluminum foil fuses in a water tampered arrangement results in lower power expenditure. The water medium also offers the advantage of generating up to three times the driving voltage compared to that in air. The dictating parameters for power consumption here are the rate of recovery of the switch and the amplitude of the commutated current during commutation in the fuse.

In the closed circuit posture the conducting switch element is a 12 inch long, cylindrical aluminum liner. The liner is completely filled with a 2 inch diameter solid paraffin plug - along the entire axial length of which runs a 150 grain piece of PETN "prima-cord." The cartridge is connected in series to the low voltage side of the clamp switch on the one end and the high side of the inductive store on the other. On detonation of the prima-cord, the action of hot explosive gases is transferred to the paraffin. During the opening process the high speed molten paraffin issues between a set of tapered polyethylene insulating rings to quench the high voltage arcing. After opening over the bending dies each stage of the switch is separated from another by the polyethylene rings; these partitions serve to insulate the respective sections of the segmented liner. The qualitative profile shown in Figure 10 portrays a mechanical response time (i.e., the explosive induction time, plus a time for elastic yielding of the aluminum liner over the bending dies) of 90 microseconds. The arc dwell time for completing current interruption depends on the cross sectional area and inductive behavior of the particular fuse configuration paralleled across the switch.

Other conventional schemes generally employed as high power circuit breakers, such as ignitron actuated "power-crowbar" techniques or ohmically vaporized shunts generally require a rather substantial power consumption. Both of these techniques are believed to be inadequate for the current parameters considered here. Ignitron circuits are generally rather expensive, electronically complex arrays which can induce significant spurious noise into the current profile. Vaporizing shunt devices can expend upwards of 50% of the system's initially carry the large currents.

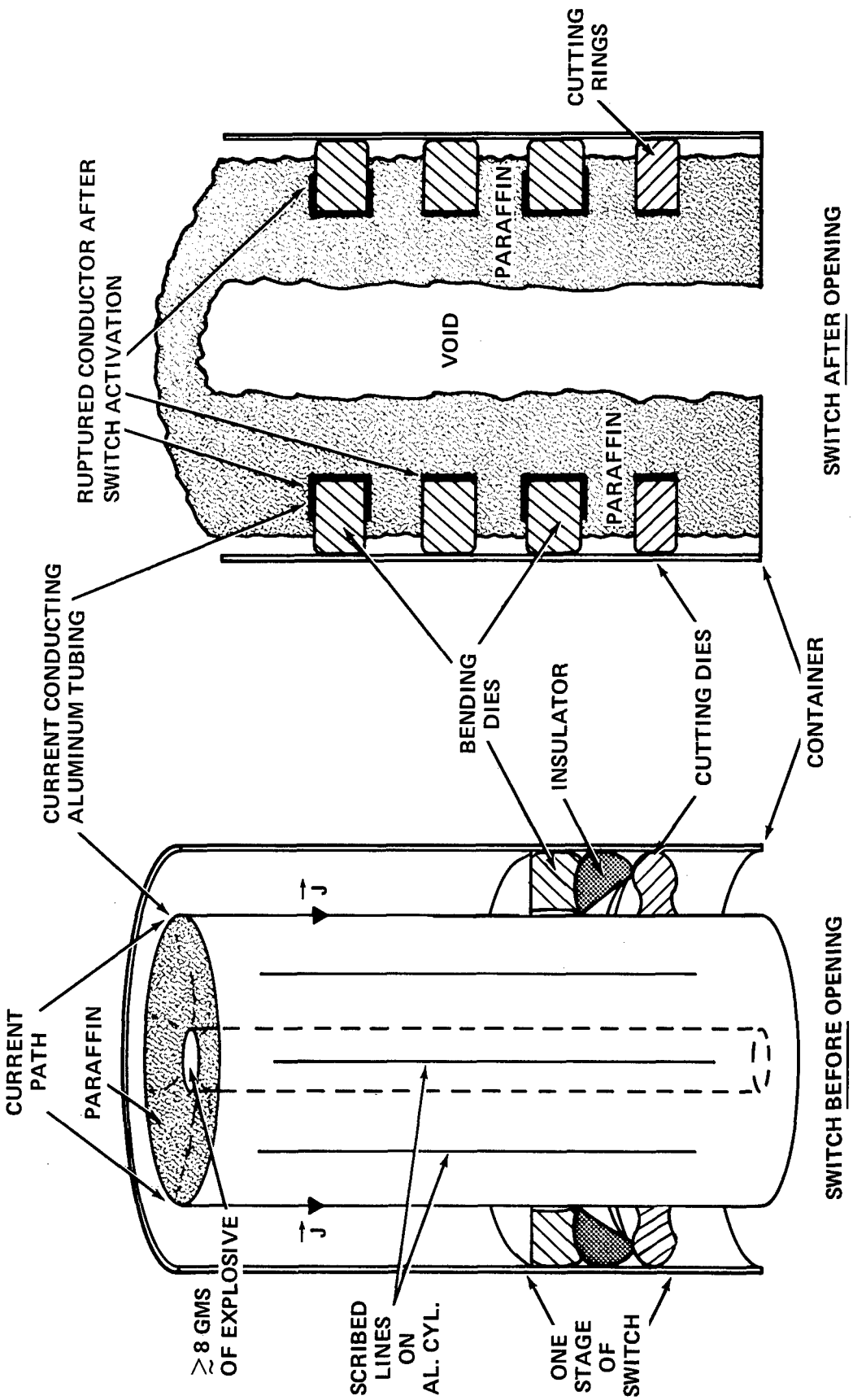

FIGURE 12 EXPLOSIVELY ACTUATED OPENING SWITCH MODULES USED TO DISENGAGE CAPACITOR ASSEMBLY. (REF. 28)

ELECTRODE ACCELERATOR CONFIGURATIONS. Figure 13 illustrates the two electrode configurations currently considered for this study. In each instance the explosive sample is extended 2.5 cm beyond the electrode ends to insure that a planar detonation front is propagating as nearly normal to incident to the electrode entry as is possible. The explosive extensions also serve to establish baselines for the camera measurements. The planar configuration affords a simpler analysis because the electric field distribution in the rectangular shaped reaction zone is uniform and one dimensional. For this configuration the camera will be able to directly track the detonation front down the length of explosive slab using standard optical techniques. The principal concern with this geometry lies with the risk of "current channeling" (arcing) along the boundary walls of the accelerator. The electrode configuration to be employed first is a coaxial geometry. Here the explosive conduction path is an annular channel. The obvious disadvantage here lies in the complication of the electric field distribution which is radially divergent. However, this geometry lends itself to direct velocity measurements. (These are of a similar nature to established cylinder tests.) The annular geometry (Figure 14) does not present conditions for current arcing to occur. To assess detonation velocity enhancement, a high speed image-converter camera is employed to track the expansion rate of the outer cylinder wall. These results are compared against the "power-off" situation, for reference.

EXPLOSIVE CONTAINMENT-CHAMBER. The entire explosive electrode assembly is housed in a forty foot steel explosion chamber which has been evacuated to 1 torr pressure for sound abatement of the blast wave. Figure 15 is a top view of the entire experimental layout as it presently exists.

Diagnostic Techniques

OPTICAL TRACKING TO DETERMINE THE DETONATION VELOCITY. The evoluation of detonation enhancement will be followed with an ultra-high speed image-converter camera employing standard time-sweep techniques. For the sequence of experiments using the cylindrical electrode setup, the optical diagnostics are performed while operating in the streak mode at a recording rate of 10 mm/μsec. With a possible resolution of 200 nanoseconds, the exposure time is 10 microseconds during which the detonation front travels about 8.8 cm. The recording sequence tracks the progress of the detonation front along the length of the outer electrode surface as schematically depicted in Figure 16. A Pockel cell setup provides time-marks.

The longitudinal length of the outer cylindrical electrode surface is vertically aligned with the primary focal plane of the camera optics. The resultant image is optically restricted to a defining slit aperature allowing only a thin section of the outer cylinder wall to be observed. Frontal illumination is provided by a 20 microseconds exploding wire source. This, in turn, is reflected off the front-most section of the outer circular cylinder wall, a portion of which is subtended at the slit to be re-imaged and amplified for recording. As the outer cylinder wall radially flares, the

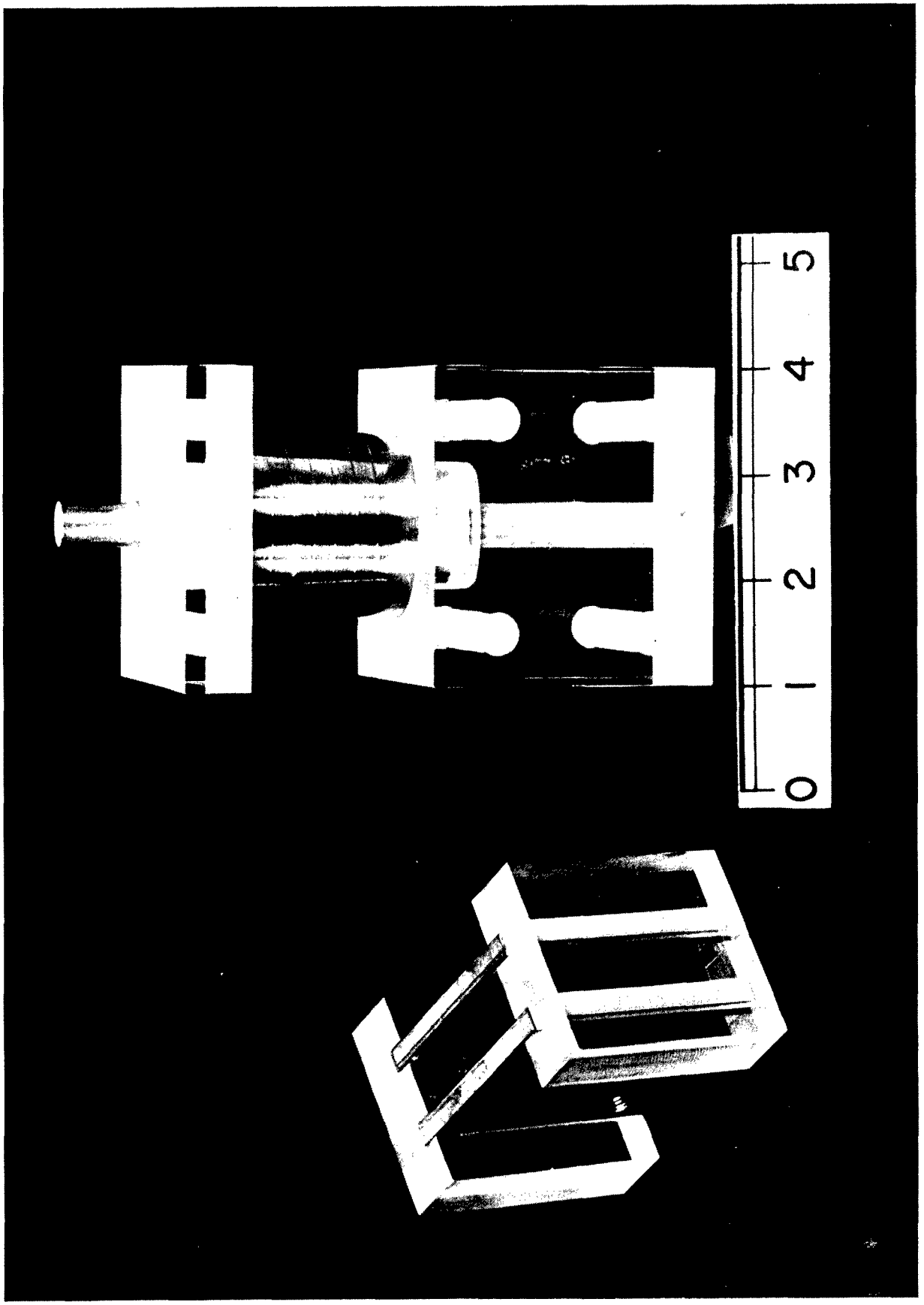

FIGURE 13 ELECTRODE ASSEMBLY: ANNULAR-COAXIAL GEOMETRY

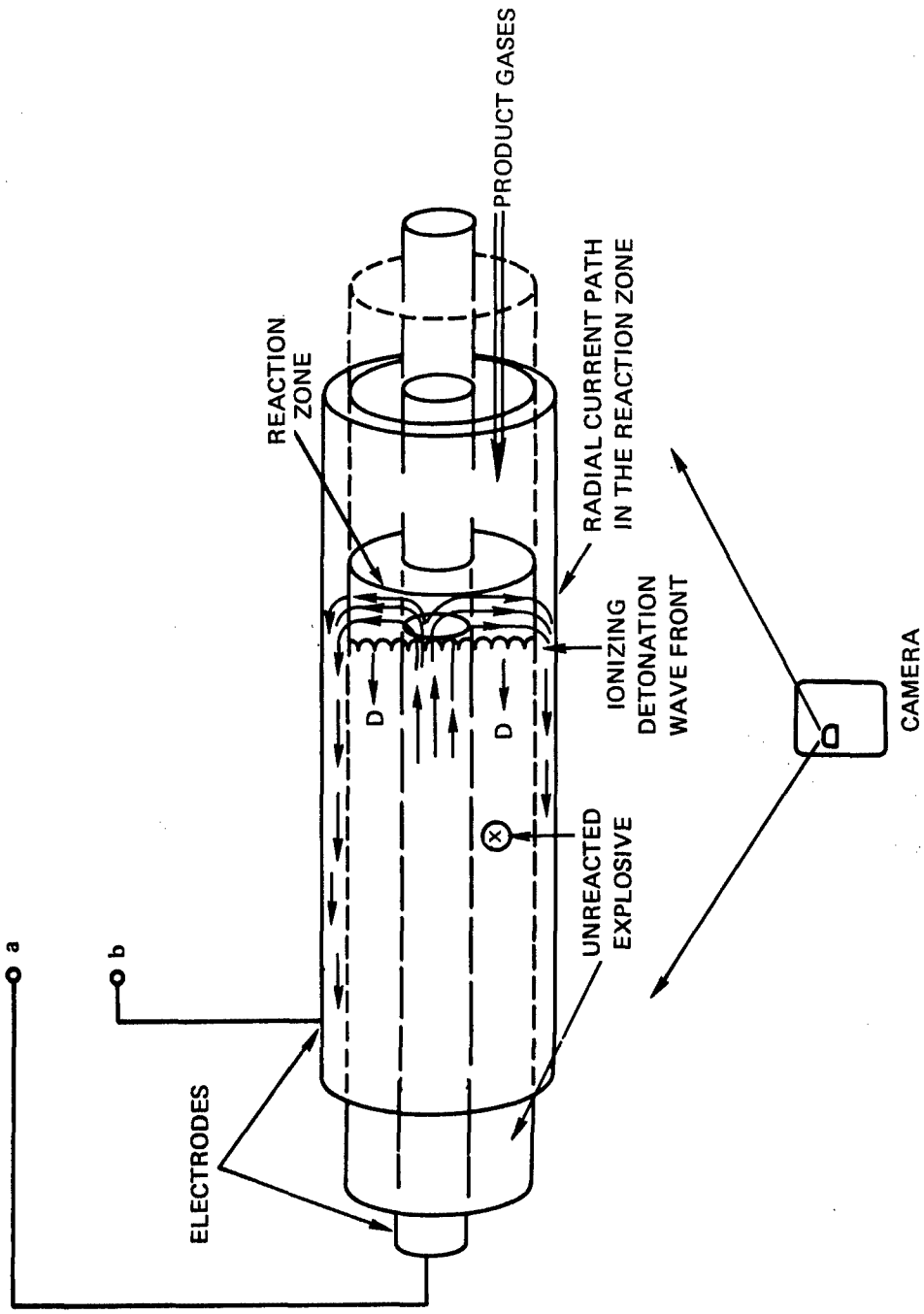

FIGURE 14 ELECTRICAL-TO-CHEMICAL ENERGY COUPLING IN THE CYLINDRICAL ELECTRODE CONFIGURATION.

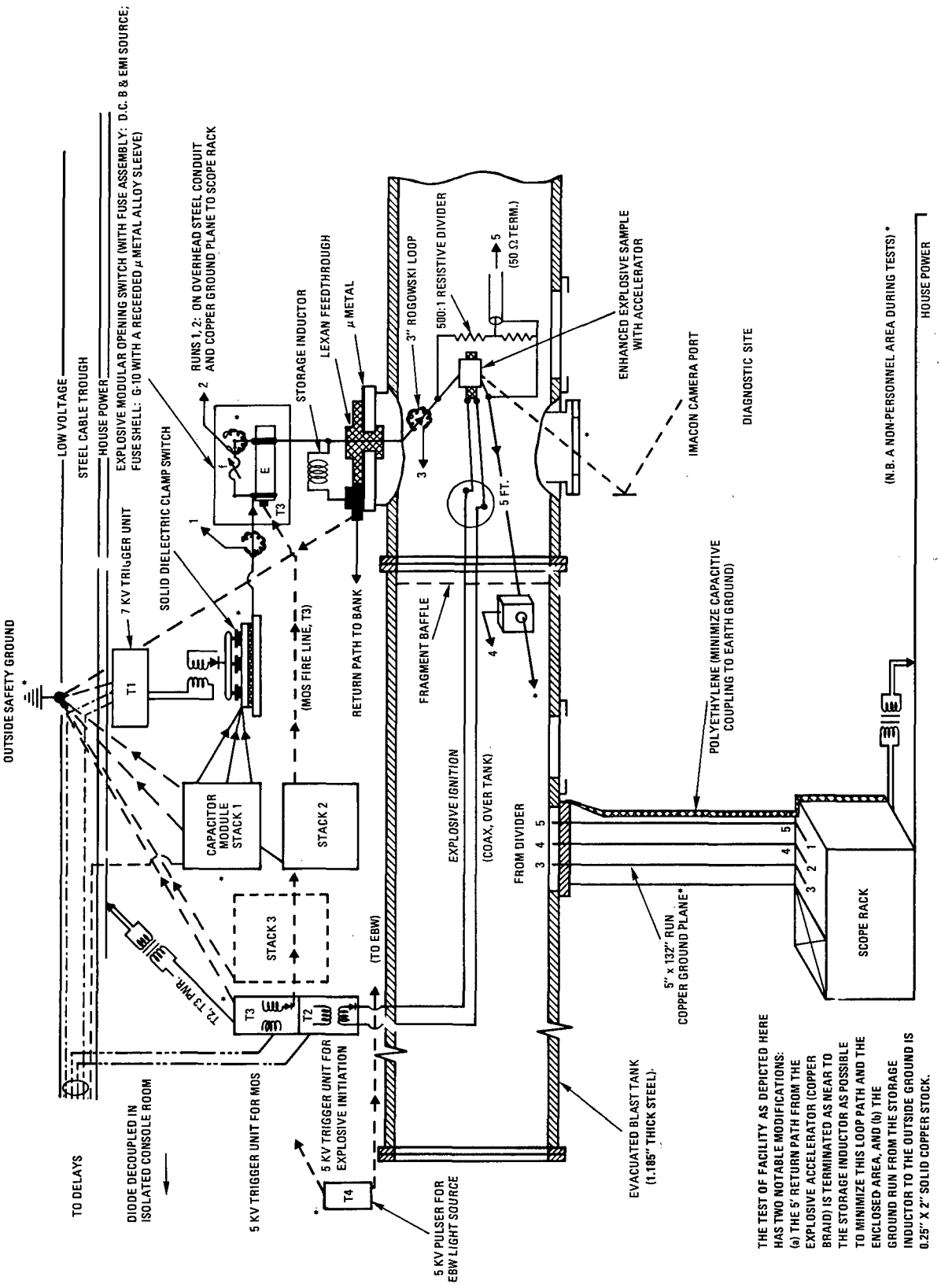

FIGURE 15. TEST FACILITY

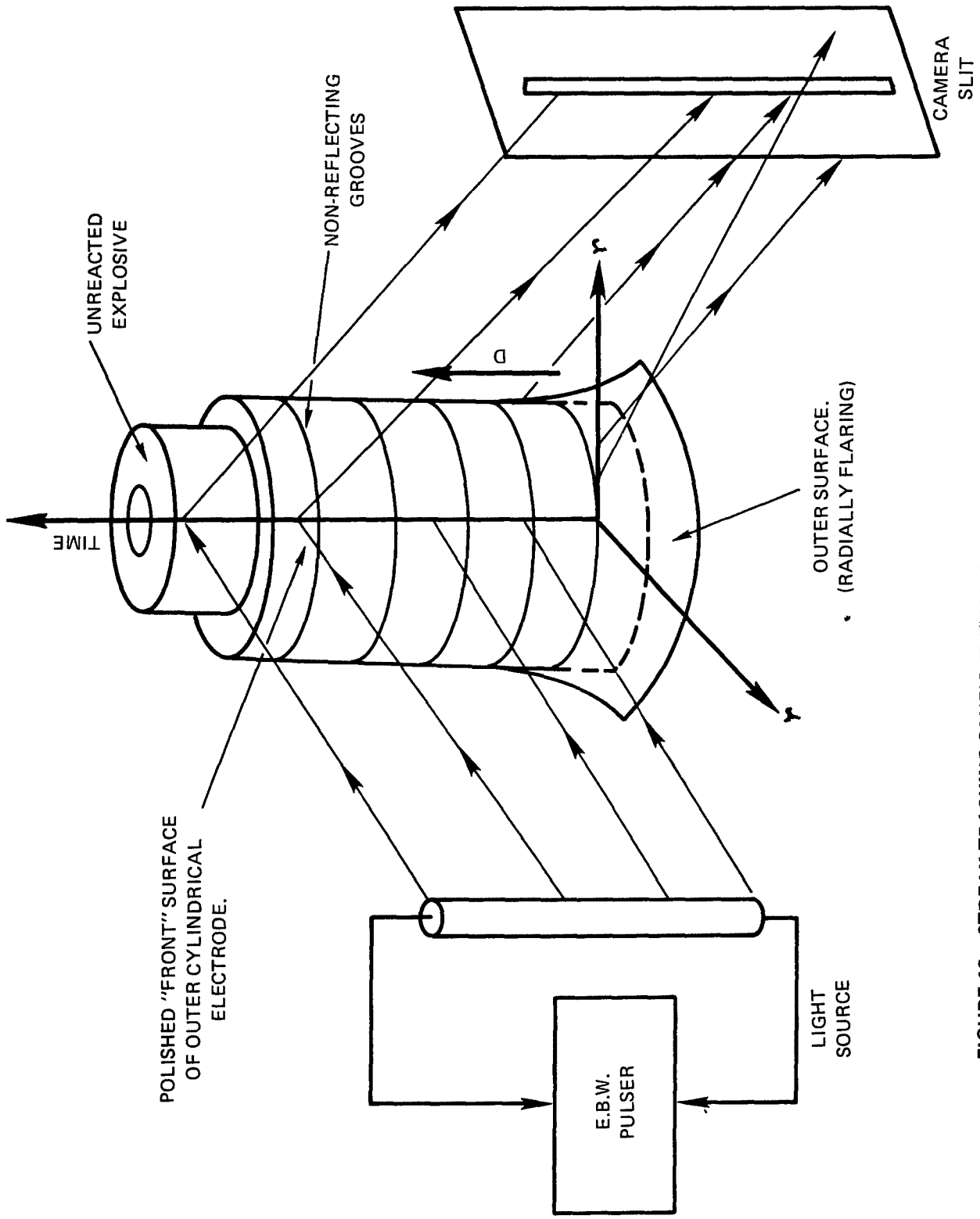

FIGURE 16 STREAK TRACKING CONFIGURATION OF THE OUTER CYLINDRICAL ELECTRODE, SET UP TO FOLLOW THE EVOLUTION OF DETONATION.

reflected light is no longer aligned with the slit. The subsequent "smear" thus serves to delineate the rate at which the cylinder wall moves once the camera has been calibrated. The cylinder wall has been optically polished and micro-grooved every 5.0 mm down the vertical extent of the cylinder wall. These precisioned markings serve to determine the spatial extent along the run of the cylinder wall to within tolerances of one-thousandth of an inch. The detonation velocity of PBX 9404 incased inthe cylinder can be accurately measured prior to an "enhanced" run. The results under "power-on" conditions are then photographed and measured from the time-sweep variation in the luminosity from the reflected strip section off the cylinder wall. Subsequently, the interrupted slit image of a line in the event is swept across the film emulsion at a uniform rate thus producing a record of light intensity distribution against a known time base. This allows the shock velocity and the duration to be directly resolved from a time-swept photograph.

An alternate measurement on the coaxial electrode is to measure the radial expansion of the cylindrical electrodes. Measurements would be made when the electrodes are energized and when they are not. These two types of measurements allow for relative comparisons so enhancement of outer electrode velocity can be easily assessed.

ELECTRICAL MEASUREMENTS. Monitoring the current flow through the electrodes is accomplished by use of a conventional 0.2-10 kHz integrating Rogowski Coil with a 0.5 mV/A sensitivity and a 10 nsec. to-peak response characteristic. The device is designed and shielded to be sufficiently uncoupled from any external stray noise sources such as, inductive pick-up from the storage coil. Calibration has been made against a constant current generator with the same range of signal characteristics as those expected to be measured.

Voltage measurements are made using a fully calibrated resistive voltage divider having a characteristic response time on the order of about 100 nsec. The energy introduced into the detonation wave is determined from a Tektronix 556 synchronized scope trace by the integration

$$W = \int_0^{\tau} I(t)\, V(t)\, dt \quad , \text{ in time } = \tau .$$

CONDUCTIVITY MEASUREMENTS. From measured values of the voltage drop across the detonation-electrode assembly and of the current flowing through it, the total resistance can be deduced as the ratio of the two.[29] If it is tacitly assumed that the only significant region of current flow is through the reaction zone of the detonation process, an average value of conductivity can be directly obtained. Unfortunately, conductivity values inferred from such direct methods yield meaningful results only in special circum-

[29] Huddlestone, R. H. and Leonard, S. L., Eds., Plasma Diagnostic Techniques, Academic Press, Inc., New York, pp. 19-27, 1965.

stances and should be regarded with some trepidation when applied to this experimental configuration. On the assumption that voltage corrections for inductive contributions from the external circuitry can be made, further complications due to the possible existence of a resistive layer caused by possible thermal[25] and field emission effects[30] in the immediate vicinity of the electrode are likely (even under high current conditions). The ablative effects of the detonation wave as it sweeps past the electrodes can produce a result something like a Child-Langmire effect.[28] The presence of metal particles from the electrodes serve to increase the conductivity, locally altering the electric field distribution, and consequently redistributing the potential across the electrode pair. Experimental evidence of these localized effects as produced by condensed explosive detonations are described in the paper by Datsenko, Korol'kov, Kransnov and Mel'nikov.[22] The presence of the metal particles form in a layer near the surface of the electrodes.

Ordinarily, the features of the experimental simplicity and very localized sampling characteristics would recommend electro-static probes as a highly viable technique for conductivity measurements. However, the effects of a highly collision-dominated medium, as in the case of the high pressure regime considered here, has a two-fold consequence. First, these effects complicate probe analysis, especially for non-equilibrium situations. Second, for such high plasma parameter regemes (i.e., $g \sim 12$) the probe itself has strong perturbational effects due to the negligible sheath formation under such conditions.[30,31] Finally, the latest pulsed probe techniques, even those employed in rapid fluctuation measurements, have insufficient sampling resolution (on the order of ~0.1 ms.).[32] In conclusion, Langmuir type probe techniques may not be reliable for fast non-equilibrium high pressure situations and the error would be significant when some fraction of the current discharge flows into the probe.[30] The use of various other electrostatic types of probes under very low current conditions have been traditionally employed in attempting to measure conductivity profiles in a detonation wave. In these probe systems where the instrument is mounted "on axis" and normal to the detonation front, measurements are obtained as the detonation is swept over them. These have met with varying degrees of success; the perturbational influence of the probe on the detona-

[30] Huddleston, R. H. and Leonard, S. L., Eds., Plasma Diagnostic Techniques, Academic Press, Inc., New York, pp. 113-124, 151-162, 189-194.

[31] Boyd, R. F., "Probe Theory in the High Pressure Regime," Proc. Phys. Soc., (London) p. 976, July 1959.

[32] Schoenberg, K. F., "Pulsed Electrostatic Probes as a Diagnostic for Transient Plasmas," Rev. Sci., Instrum. 49 (10), p. 1377, Oct 1978.

tion wave itself, not to mention on the conductivity profile, and the accorded resolution of such schemes are being critically scrutinized at this time.

Microwave reflection techniques[33] do not appear to suffer from the major drawback of significantly perturbing the detonation process or the conductivity profile. But recently published studies on the latest known results of this method put the spatial resolution limits on the order of about 3.5 mm. Thus the probe has a time resolution equal to the space resolution divided by the detonation velocity of about 0.4 microseconds. The probe can readily be oriented radially or axially to the detonation front. The possibility of employing this technique will have to be further investigated in future work. Application of microwave-transmission techniques are ruled out since electron densities higher than 10^{14} cm^{-3} do not allow even 150 GHz microwaves to penetrate.[33] Time Domain Reflectometry is presently being investigated as a possible resistivity probe technique. The study of conductivity profiles in partially-ionized dense detonation systems warrants further investigation.

A SUMMARIZING DISCUSSION OF THE RESULTS.

The present method for electrically coupling into the explosive detonation entails passing a very high electric current pulse through it. Specifically, the injection of 170 kA will increase the conduction zone temperature - ultimately culminating in the overdriving of the explosive's detonation velocity, and subsequently, increasing the detonation pressure and rate of energy release.

The preliminary facility arrangement deploys about 100 kilojoules of electrical energy and is expected to deliver up to about 2 times the explosive's chemical release energy through joule heating, under optimum power delivery conditions. Increases in detonation velocity are to be measured by fast time-swept, photographic techniques. The current and voltage profiles are continuously monitored by employing standard diagnostic instrumentation.

The electrically-induced augmentation of the detonation wave from a condensed explosive depends primarily on the explosive's electrical properties. Briefly, these are: (a) the electrical conductivity distribution behind the detonating explosive's shock front, and (b) the breakdown voltages of the reacted gases in the detonation product zone, and of the unreacted explosive. The extent of coupling this electrical energy into the explosive depends on the impedance characterizing the LR network assembly.

The dominant mechanism attributed to the energy enhancement effects are principally ohmic in nature. The responsible impedance

[33] Funahashi, A. and Takeda, S., "Microwave Reflection Measurements of Electron Densities in Electromagnetically Driven Shock-Produced Plasmas," Journal of Applied Physics, Vol. 39, No. 4, p. 2117, March 1968.

characteristics consist of: (a) a pure resistance, which determines the extent of joule heating, principally in the reaction zone, and (b) an inductive reactance which determines the extent of inductive heating. For the particular set of experimental parameters typically attributed to chemical explosive detonation the direct ohmic heating energy release mechanism is found to be at least an order of magnitude smaller than the explosive's own chemical release energy effects. Furthermore, for the set of electrode configurations presently being used inductive heating is insignificant.

In conclusion, this program will afford the opportunity to explore the feasibility of investigating the effects of augmenting the chemical energy of a reacting explosive with some external energy source. It will provide an additional independent parameter to influence basic explosive properties. However, a number of subtasks remain to be finished prior to attempting an observation of enhancement effects. Specifically, a continued effort must be made to bring this facility closer to a fully operational status. Once this is accomplished, high current level resistance measurements must be made. Finally, a demonstration of enhancement effects will be pursued.

REFERENCES

1. Dobratz, B. M., "Properties of Chemical Explosives and Explosive Stimulants," Lawrence Livermore Laboratory Report No. UCRL-51319, Revision 1, 1974.

2. Ershov, A. P., "Ionization During Detonation of Solid Explosives," Combustion, Explosion, and Shock Waves, pp. 798-803, November - December 1975.

3. Walbrecht, E. E., "Dielectric Properties of Some Common High Explosives," PATM 1170, p. 1, April 1963.

4. Toton, E. T., "High Explosive Detonation and Electromagnetic Interaction," NSWC TR 79-205, March 1979.

5. Brish, A. A., Tarasov, M. S., and Tsukerman, V. A., "Electric Conductivity of the Explosive Products of Condensed Explosives," Soviet Physics JETP, Vol. 37, (10), No. 6, pp. 1095-1099, June 1960.

6. Jameson, R. L., Lukasik, S. J., and Pernick, B. J., "Electrical Resistivity Measurements in Detonating Composition B and Pentolite," Journal of Applied Physics, Vol. 35, No. 3, Part 1, p. 714, March 1964.

7. Hayes, B., "On Electrical Conductivity in Detonation Products," Fourth International Symposium on Detonation, p. 595, 1965.

8. Jones, M. S. and Blackman, V. H., "Parametric Studies of Explosive Driven MHD Power Generators," Symposium on the Engineering Aspects of MHD, Vol. 2, August 1964.

9. Jones, M. S., Mckinnon, C. N., and Blackman, V. H., "Generation of Short Duration Pulses in Linear MHD Generators," Proceedings of Fifth Symposium on the Engineering Aspects of MHD, MIT, April 1964.

10. Zubbov, P. I., Luk'yanchikov, L. A., and Novoselov, B. S., "Electrical Conductivity in the Detonation Zone of Condensed Explosives," Combustion, Explosion, and Shock Waves, pp. 253-256, June 1971.

REFERENCES (Cont.)

11. Allison, F. E., "Detonation Studies in Electric and Magnetic Fields," Proceedings of the Conference on Megagauss Magnetic Field Generation by Explosives and Related Experiments, 21-23 September 1965.

12. Reif, F., Statistical and Thermal Physics, McGraw-Hill Book Company, New York, pp. 531-534, pp. 580-582, 1965.

13. Dreicer, H., "Electron Collision Phenomena in Partially Ionized Gases," Phys. Rev. 117, p. 329, 1960.

14. Krall, N. A. and Trivelpiece, A. W., Principals of Plasma Physics, McGraw-Hill Book Co., Inc., New York, p. 57, 1973.

15. Zel'dovich, Ya. B. and Raizer, Yu. P., Physics of Shock Waves and High-Temperature Hydrodynamic Phenomena, Vol. 1, Academic Press, Inc., pp. 218-219, pp. 229-232, 1966.

16. Jones, M. S., Bangerter, C. D., Peterson, A. H., and Mckinnon, C. N., "Explosive Magnetohydrodynamics, AFAPL-TR 67-64, pp. 57-72, August 1967.

17. Jackson, J. D., Classical Electrodynamics, 2nd, Ed., John Wiley and Sons, Inc., pp. 471-479, 1975.

18. Sutton, G. W. and Sherman, A., Engineering Magnetohydrodynamics, McGraw-Hill Book Co., New York, pp. 125-209, and pp. 300-304, 1965.

19. Landau, L. D. and Lifshitz, E. M., The Classical Theory of Fields, 2nd. Ed., Addison-Wesley Publishing Co., Inc., Reading, Massachusetts, pp. 101-108, 1962.

20. Landau, L. D. and Lifshitz, E. M., Electrodynamics of Continuous Media, Addison-Wesley Publishing co., Inc., Reading, Massachusetts, pp. 197-212, 1960.

21. Korol'kov, V. L., Mel'nikov, M. A., and Tsyplenko, A. P., "Dielectric Breakdown of Detonation Products," Sov. Phys., Tech. Phys., Vol. 19, No. 12, p. 1569, June 1975.

22. Datsenko, V. A., Korol'kov, V. L., Krasnov, I. L., and Mel'nikov, M. A., "Dielectric Breakdown of Detonation Products," Sov. Phys, Tech. Phys.. 23 (1) p. 33, Jan 1978.

23. Greenwood, A. and Lee, T. H., "Generalized Damping Curves and Their Use in Solving Power-Switching Transients," Trans, IEEE, Vol. 82, Part III, p. 527, 1963.

REFERENCES (Cont.)

24. Chu, B. T., "Thermodynamics of Electrically Conducting Fluids," Physics of Fluids, Vol. 2, No. 5, p. 473, Oct 1959.

25. Salge, J. and Braunsberger, U., "Inductive Energy Storage Systems Applied for the Extension of Current Pulse-Duration of Capacitor Banks," Symp. Fusion Technology, 7th, Grenoble, Oct 1972.

26. Griem, H. R. and Loveberg, R. H., Eds., Methods of Experimental Physics; Plasma Physics, Vol. 9, Part A, Academic Press, Inc., New York, pp. 198-199, 1970.

27. Ford, R. D. and Young, M. P., "Chemical-Detonator Solid-Dielectric Switches for Starting and Clamp Applications," Proceedings of the 8th Symp. on Fusion Tech., EUR 5182e, Sep 1974.

28. Ford, R. D. and Vithovitsky, I. M., "Explosively Activated 100 kA Opening Switch for High Voltage Application," NRL Report No. 3561, July 1977.

29. Huddlestone, R. H. and Leonard, S. L., Eds., Plasma Diagnostic Techniques, Academic Press, Inc., New York, pp. 19-27, 1965.

30. ibid., pp. 113-124, pp. 151-161 and pp. 189-194.

31. Boyd, R. F., "Probe Theory in the High Pressure Regime," Proc. Phys. Soc., (London) p. 976, July 1959.

32. Schoenberg, K. F., "Pulsed Electrostatic Probes as a Diagnostic for Transient Plasmas," Rev. Sci., Instrum., 49 (10), p. 1377, Oct 1978.

33. Funahashi, A. and Takeda, S., "Microwave Reflection Measurements of Electron Densities in Electromagnetically Driven Shock-Produced Plasmas," Journal of Applied Physics, Vol. 39, No. 4, p. 2117, March 1968.

APPENDIX A

INDUCED OHMIC HEATING EFFECTS

An estimate of the "induced" ohmic heating effects are readily attained for the 1.7×10^5 A current flow in the cylindrically concentric, electrode pair. The effect primarily depends on the magnitude and rate of induced magnetic field diffusion into the conductive region of the detonation process. These values are based on the magnetic Reynold number[A1] R_m and magnetic diffusion time τ. To make the analysis more tractible, the conductivity $\eta(\xi)$ will be assumed constant across the reaction zone (i.e. $\frac{d\eta}{d\xi} = 0$).

Upon insertion of Equation (12) into Faraday's Induction Equation,[A2] in R.M.K.S. units,

$$\frac{\partial \vec{B}}{\partial t} = - \left(\vec{\nabla} x \vec{E}\right) \tag{A.1}$$

$$= - \vec{\nabla} \times \left(\eta \vec{J} + \vec{D} x \vec{B}\right) . \tag{A-2}$$

The curl of Ampere's Law transforms

$$\vec{\nabla} x \left[\nabla x \vec{B} = \mu_o \vec{J}\right] \tag{A.3}$$

into

$$-\vec{\nabla}^2 \vec{B} = \frac{\mu_o}{\eta} \vec{\nabla} \times \vec{J} \quad . \tag{A.4}$$

Since there is no curvature,

$$\nabla(\nabla \cdot B) = 0. \tag{A.5}$$

[A1] Sutton, G. W. and Sherman, A., Engineering Magnetohydrodynamics, McGraw-Hill Book Co., New York, pp. 125-209, and pp. 300-304, 1965.

[A2] Jackson, J. D., Classical Electrodynamics, 2nd, Ed., John Wiley and Sons, Inc., pp. 471-479, 1975.

Relative to the laboratory frame of reference Equation (A.2) gives[A2]

$$\frac{\partial \vec{B}}{\partial t} = \frac{\eta}{\mu_o} \nabla^2 \vec{B} + \vec{\nabla} \times (\vec{D} \times \vec{B}) \qquad \text{(RMKS)} \; . \qquad \text{(A.6)}$$

The first term on the R. H. S. is the familiar field diffusion term; the second term is a convective term, important for moving resistive fluids. If the field lines penetrate the conduction zone fast enough, $\frac{1}{\tau_B} \equiv \frac{\eta}{\mu_o \ell^2}$, the induced field effects cause ohmic heating of the fluid. This energy is due to the presence of the $\vec{B}$ field; the energy lost per cm^3 in a time t is $(\eta j^2)t$.[A3] By Ampere's law

$$\vec{j} = \frac{1}{\mu_o} \vec{\nabla} \times B \sim \frac{B}{\mu_o \ell} \; . \qquad \text{(A.7)}$$

The energy dissipation is

$$(\eta j^2) t \Big|_{\tau_B} = \frac{\eta}{2} \left(\frac{B}{\mu_o \ell} \right)^2 \cdot \frac{\mu_o \ell^2}{\eta} \qquad \text{(A.8)}$$

or

$$= \frac{1}{2\mu_o} B^2, \; \mu_o = 1.26 \times 10^{-6} \text{ Henry/m} \; . \qquad \text{(A.9)}$$

The magnetic Reynolds number[A1] R_m (a comparison of the R.H.S. terms in Equation (A6)) will indicate how easily the fluid slips through the magnetic field. Relative to the laboratory frame, the ratio of these terms is

$$R_m = \frac{D \; B/\ell}{\eta/\mu_o \cdot B/\ell^2} = \frac{\mu_o D \ell}{\eta} \; . \qquad \text{(A.10)}$$

For our explosive detonation situation where a selected maximum resistivity, $\eta_{max} = 10^3 \; \Omega \cdot m$, and D is the PBX 9404 detonation velocity

$$D = 8.8 \times 10^3 \text{ m/sec}$$

$$\ell = 1.5 \; 10^{-3} \text{ m (width of idealized conduction zone)}$$

[A3] Griem, H. R., and Loveberg, R. H., Eds., Methods of Experimental Physics; Plasma Physics, Vol. 9, Part A, Academic Press, Inc., New York, pp. 403-418, 1970.

$$R_m = \frac{(1.26\ 10^{-6})(8.8\times10^{3})(1.5\ 10^{-3})}{10^{3}} \sim 10^{-8} \quad . \qquad (A.11)$$

For $R_m << 1$, therefore, some diffusion of the induced magnetic field lines across the conductive zone of the detonation wave is anticipated. To ascertain how significant the effect can become, the most optimistic case would be $i = i_{max} = .17$ MA. This, however, assumes a rectangular current pulse about 10 microseconds long, where, in fact, the actual current situation is $i = i_{max} \exp\left(\frac{-R}{L_s}\tau\right)$; and consequently the magnetic field $B \approx B_{max} \exp\left(\frac{-R}{L_s}\tau\right)$ where, R as a function of the conduction zone resistivity $\eta(\varepsilon)$, is assumed constant. In the 0.17 MA situation for the cylindrical configuration with $r_1 = 0.7$ cm.

$$B_{max} = \left(\frac{\mu_o\, i_{max}}{2\pi r_1}\right) = 4.87 \text{ Tesla} \quad . \qquad (A.12)$$

From Equation (A.9), the maximum energy dissipation per cm^3 given by

$$(\eta j^2)\tau_{max} = \frac{1}{2\mu_o}\ \frac{\mu_o i_{max}^2}{2\pi r} = \frac{\mu_o i_{max}^2}{8\pi^2 r^2} \quad \text{(per unit volume)} \quad . \qquad (A.13)$$

The total energy available to the 5 cm long coaxial electrode is

$$U = \int dU = \int_{\Gamma} (\eta j^2)_{\tau} d\Gamma = \frac{\mu_o i^2 L}{4\pi} \ln\left(\frac{r_1}{r_o}\right), \qquad (A.14)$$

where the volume Γ is a cylindrical shell 5 cm long, with radii $r_1/r_o = 2.0$. Therefore, using the coaxial electrode pair

$$U = \frac{(1.26 \times 10^{-6}\ H/m)(1.7 \times 10^{5}\ A)^2\ (0.05\ m)}{4(3.141)} \quad (0.69)$$

$$\equiv 101 \text{ joule} \quad . \qquad (A.15)$$

This energy release is $\sim 3 \times 10^3$ smaller than that of the total chemical release energy of the detonated charge. What is significant here, however, is the implications associated with Equation (A.7). Since $R_m << 1$, the diffusion term is dominant in Equation (A.6).

From Equation (A.6) the magnetic diffusion time is given by

$$\tau_B = \mu_o \sigma \ell^2, \quad \text{where } \ell \text{ is a length characteristic of the spatial variation of B relative to an observer in the conduction zone.}$$

If τ_B is defined as the total time for the field to diffuse through the conduction zone as it traverses the accelerator electrodes, the power dissipated goes into joule heating. With the present experimental arrangement, the electrode length L = 0.05 m; taking a nominal bulk conductivity value $\sigma = 10^2$ mho/m (cf Figure 2),

$$\begin{aligned} \tau_B &= \mu_o \sigma L^2 \ (\text{sec}) \\ &= (1.25 \times 10^{-6})(10^2)(0.05)^2 \\ &= 0.31 \ \mu\text{s}. \end{aligned} \tag{A.16}$$

The detonation "time-of-flight" through the 0.05 m electrodes is

$$\tau_D \ (= L/D) = \frac{0.05 \text{ m}}{8.8 \times 10^3 \text{ m/sec}} = 5.7 \ \mu\text{sec} . \tag{A.17}$$

Consequently, the "interaction parameter"

$$N \equiv \frac{\tau_B}{\tau_D} \quad (\neq Rm) = 0.05 . \tag{A.18}$$

N < 1 implies that there is sufficient time for the annihilation of the magnetic flux lines to produce the ohmic heating. Equation (A.6) implies that for $B_G \sim .25$ MG (e.g., a multi-turned solenoid about a dielectric shell, used as an electrode) the induction heating energy would be comparable to the chemical release energy of the detonation, the explosive reaction zone acting as the secondary coil of a transformer.[A4]

[A4] Hooke, W., and Caldirola, P., Eds., Symp. on Plasma Heating and Injection, International School of Plasma Physics, Varenna, Italy, pp. 61-72, Sep 21 - Oct 1972.

DISTRIBUTION

	Copies
Chief of Naval Material Washington, DC 20360	1
Director Headquarters Naval Material Command Attn: MAT-08T2 Washington, DC 20360	1
Defense Technical Information Center Cameron Station Alexandria, VA 22314	12
Commander Naval Sea Systems Command Attn: SEA-03B	1
SEA-62R (W. Blaine)	1
SEA-62R32 (G. Edwards)	1
SEA-99612 (Technical Library)	2
Washington, DC 20360	
Commander Naval Air Systems Command Attn: AIR-350 (H. Benefiel)	1
AIR-440 (G. Heiche)	1
AIR-00D4 (Technical Library)	1
Department of the Navy Washington, DC 20362	
Chief of Naval Research Office of Naval Research Attn: ONR-432 (R. Miller)	1
ONR-400 (J. Satkowski)	1
ONR-412 (R. Junker)	1
Technical Library	1
800 N. Quincy Street Arlington, VA 22217	

	Copies
Director Office of Naval Technology Attn: J. Enig	1
E. Zimet	1
Arlington, VA 22217	
Commander Naval Weapons Center Attn: A. Addison	1
A. Adicoff	1
D. B. Amster	1
G. Green	1
T. Joyner	1
D. Mallory	1
China Lake, CA 93555	
Commander Naval Research Laboratory Attn: J. Aviles	1
J. Ford (B. 704T)	1
A. Stolovy	1
I. Vitkovitsky (B. 71)	1
Technical Library	1
Washington, DC 20375	
Commanding Officer U. S. Army Armament Research and Development Command Attn: R. Walker	1
N. Slagg	1
Technical Library	1
Dover, NJ 07801	
Commanding Officer Aberdeen Research and Development Center Attn: Technical Library	1
Aberdeen, MD 21005	

DISTRIBUTION (Cont.)

	Copies
Director Air Force Office of Scientific Research	
Attn: Col. R. Detweiler	1
Col. H. Bryan	1
T. Walsh	1
Library	1
Bolling Air Force Base Washington, DC 20332	
Commanding Officer Naval Ordnance Station	
Attn: Research and Development Department	1
Technical Library	1
Indian Head, MD 20640	
Commander Air Force Armament Development and Test Center	
Attn: Lt. Col. Scott	1
Eglin Air Force Base, FL 32542	
F. J. Seiler Research Laboratory	
Attn: Col. B. Loving	1
U. S. Air Force Academy Colorado Springs, CO 80840	
Lawrence Livermore National Laboratory	
Attn: H. Kruger	1
M. Finger	1
B. Hayes	1
E. Lee	1
R. McGuire	1
Technical Library	1
University of CAlifornia Livermore, CA 94550	

	Copies
Director Los Alamos National Laboratory	
Attn: G. Wackerly	1
R. Rogers	1
W. Davis	1
G. Hughes	1
C. Max Fowler (M-6)	1
J. Shaner	1
D. Erickson (M-6)	1
W. Sargeant	1
J. Huff	1
T. Frank	1
T. McDonald	1
Technical Library	1
Los Alamos, NM 87544	
Director Johns-Hopkins Applied Physics Laboratory	
Attn: S. Koslov	1
Technical Library	1
Johns-Hopkins Road Laurel, MD 20707	
Commander Harry Diamond Laboratory	
Attn: R. K. Warner (Br. 21100)	1
R. Garver	1
W. Gray	1
W. Petty	1
Technical Library	1
2800 Powder Mill Road Adelphi, MD 20783	
University of Maryland	
Attn: Plasma Physics Dept.	1
Technical Library	1
College Park, MD 20740	

DISTRIBUTION (Cont.)

	Copies
Director Defense Advance Research Projects Agency Washington, DC 20301	1
Scientific Research Associates, Incorporated Attn: B. Weinberg P. O. Box 498 Glastenbury, CT 06033	1
Science Applications Attn: W. Chadsey 8330 Old Courthouse Road Suite 510 Vienna, VA 22180	1
Director Sandia National Laboratories Attn: D. Hayes J. Kennedy Technical Library P. O. Box 5800 Albuquerque, NM 87115	1 1 1
Honeywell Defense Attn: P. DiBona 600 2nd Street N. Hopkins, MN 55343	1
Library of Congress Attn: Gift and Exchange Division Washington, DC 20540	4
Maxwell Laboratories, Inc. Attn: P. Elliot 8835 Balboa Avenue San Diego, CA 92123	1

	Copies
Department of Electrical Engineering Bell Hall Attn: A. Gilmour, Jr. State University of New York at Buffalo Buffalo, NY 14214	1
Georgia Institute of Technology Georgia Tech. EES; RAIL/RED Attn: D. Ladd Atlanta, GA 30332	1
AVCO Everett Research Laboratory Attn: C. Pike 2385 Revere Beach Parkway Everett, MA 02149	1
Physics International Co. Attn: A. Rutherford 2700 Merced Street San Leandro, CA 94577	1